Epithelial apoptotic pattern emerges from global and local regulation by cell apical area

Victoire M.L. Cachoux, Maria Balakireva, Mélanie Gracia, Floris Bosveld, Jesús López-Gay, Aude Maugarny, Isabelle Gaugué, Florencia Di Pietro, Stéphane Rigaud, Lorette Noiret, et al.

▶ To cite this version:

Victoire M.L. Cachoux, Maria Balakireva, Mélanie Gracia, Floris Bosveld, Jesús López-Gay, et al.. Epithelial apoptotic pattern emerges from global and local regulation by cell apical area. Current Biology - CB, 2023, 10.1016/j.cub.2023.09.049 . hal-04238055

HAL Id: hal-04238055
https://hal.science/hal-04238055
Submitted on 11 Oct 2023

Article

Current Biology

Epithelial apoptotic pattern emerges from global and local regulation by cell apical area

Graphical abstract

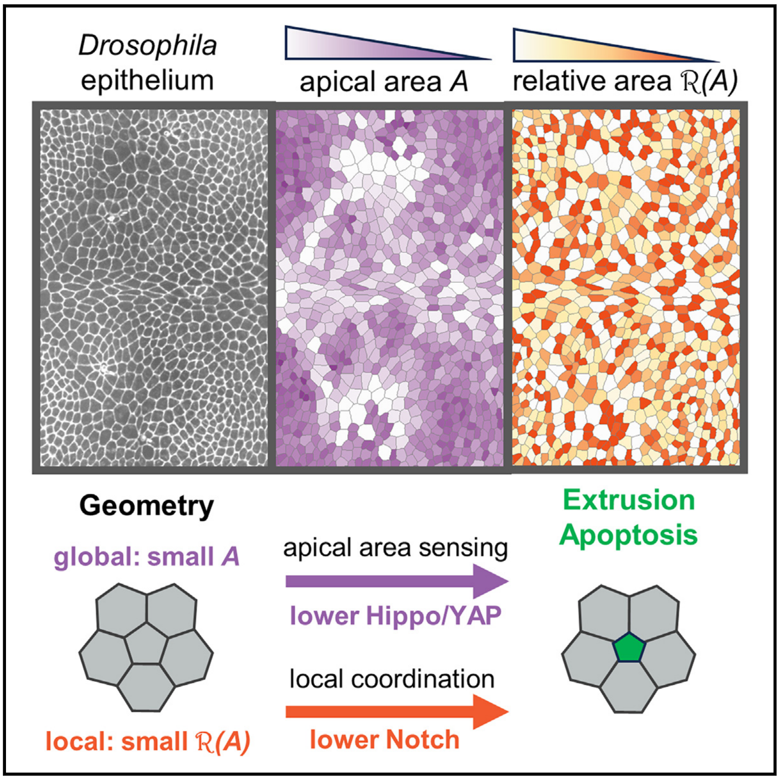

Highlights

- Cell probability to die increases with decreasing apical area
- For a given apical area, cell probability to die increases with bigger neighbors
- Regulation of apoptosis by cell apical area depends on Hippo/YAP activity
- By preventing apoptotic clusters, Notch influences the relative area regulation

Authors

Victoire M.L. Cachoux, Maria Balakireva, Mélanie Gracia, ..., Lorette Noiret, Boris Guirao, Yohanns Bellaïche

Correspondence

boris.guirao@curie.fr (B.G.),
yohanns.bellaiche@curie.fr (Y.B.)

In brief

In developing *Drosophila* epithelial tissue, Cachoux, Balakireva et al. find that apoptosis is more likely to occur in cells that harbor a small apical area and are surrounded by larger neighbors. Regulation of apoptosis by these global and local geometrical factors depends on the Hippo/YAP and Notch pathways, respectively.

Cachoux et al., 2023, Current Biology *33*, 1–20
November 20, 2023
https://doi.org/10.1016/j.cub.2023.09.049

Please cite this article in press as: Cachoux et al., Epithelial apoptotic pattern emerges from global and local regulation by cell apical area, Current Biology (2023), https://doi.org/10.1016/j.cub.2023.09.049

Current Biology

CellPress

Article

Epithelial apoptotic pattern emerges from global and local regulation by cell apical area

Victoire M.L. Cachoux,[1,2] Maria Balakireva,[1,2] Mélanie Gracia,[1] Floris Bosveld,[1] Jesús M. López-Gay,[1] Aude Maugarny,[1] Isabelle Gaugué,[1] Florencia di Pietro,[1] Stéphane U. Rigaud,[1] Lorette Noiret,[1] Boris Guirao,[1,3,*] and Yohanns Bellaïche[1,3,4,5,*]

[1]Institut Curie, Université PSL, Sorbonne Université, CNRS UMR3215, INSERM U934, Genetics and Developmental Biology, 75005 Paris, France

[2]These authors contributed equally

[3]Senior author

[4]X (formerly Twitter): @bellaiche_y

[5]Lead contact

*Correspondence: boris.guirao@curie.fr (B.G.), yohanns.bellaiche@curie.fr (Y.B.)

https://doi.org/10.1016/j.cub.2023.09.049

SUMMARY

Geometry is a fundamental attribute of biological systems, and it underlies cell and tissue dynamics. Cell geometry controls cell-cycle progression and mitosis and thus modulates tissue development and homeostasis. In sharp contrast and despite the extensive characterization of the genetic mechanisms of caspase activation, we know little about whether and how cell geometry controls apoptosis commitment in developing tissues. Here, we combined multiscale time-lapse microscopy of developing *Drosophila* epithelium, quantitative characterization of cell behaviors, and genetic and mechanical perturbations to determine how apoptosis is controlled during epithelial tissue development. We found that early in cell lives and well before extrusion, apoptosis commitment is linked to two distinct geometric features: a small apical area compared with other cells within the tissue and a small relative apical area with respect to the immediate neighboring cells. We showed that these global and local geometric characteristics are sufficient to recapitulate the tissue-scale apoptotic pattern. Furthermore, we established that the coupling between these two geometric features and apoptotic cells is dependent on the Hippo/YAP and Notch pathways. Overall, by exploring the links between cell geometry and apoptosis commitment, our work provides important insights into the spatial regulation of cell death in tissues and improves our understanding of the mechanisms that control cell number and tissue size.

INTRODUCTION

In living organisms, the number of cells is regulated by the balance between cell proliferation and cell loss. The acquisition of size and shape of developing organisms, as well as adult tissue homeostasis, relies on this crucial balance.[1] In epithelial tissues, aberrant proliferation can drive tumor growth, whereas excessive cell death can jeopardize their integrity.[2,3] Numerous studies have shown that geometrical factors, including cell size and shape, are key to regulate cell proliferation and thus tissue development and homeostasis.[4–7] In sharp contrast, our understanding of how geometrical factors may control cell death is lagging behind, impeding the integrated analysis of the regulation of cell number, size, and shape in tissues.

Apoptosis is a major form of programmed cell death during development. It is a physiological, orderly process involving the activation of the cysteine-aspartic protease caspase and marked by cell shrinkage, chromatin condensation, and membrane blebbing.[8–10] The signaling pathways controlling apoptosis have been extensively characterized during development.[9,10] Furthermore, studies in epithelial tissues have defined how caspase activation leads to the remodeling of the cytoskeleton and cell adhesion to promote the apical or basal extrusion of apoptotic cells.[11–20] As such, epithelial apoptosis involves both the apoptotic cell and its direct surroundings, generating mechanical forces, cell rearrangements, or deformations that remodel the apoptotic cell environment.[12–14,16,18,20,21] By doing so, apoptosis can contribute to fusing cell layers, tissue morphogenesis, and compensatory cell proliferation,[22–29] and it is proposed to modulate tissue mechanical properties.[30] Aside from the signaling pathways triggering apoptosis, recent studies suggested that epithelial apoptosis could arise from the biophysical regulation linked to tissue "crowding" and resulting stress. In particular, ectopic mechanical compression, local topological defects, and genetically induced mechanical cell competition have been shown to promote cell apoptosis.[31–37] However, these regulatory mechanisms have not explained the spatiotemporal distribution of apoptosis during development. More generally, how biophysical factors control apoptosis, a key regulator of growth, morphogenesis, and homeostasis of tissues, remains largely unknown.

To identify the factors controlling epithelial apoptosis *in vivo*, we used the *Drosophila* pupal dorsal thorax, or notum, as a model system. This monolayered epithelial tissue is formed around 6 h after pupa formation (hAPF) by the fusion of the two wing imaginal discs along the dorsal midline[38] (Figures 1A and S1A). The pupal notum is composed of more than 10,000 cells that undergo several

Please cite this article in press as: Cachoux et al., Epithelial apoptotic pattern emerges from global and local regulation by cell apical area, Current Biology (2023), https://doi.org/10.1016/j.cub.2023.09.049

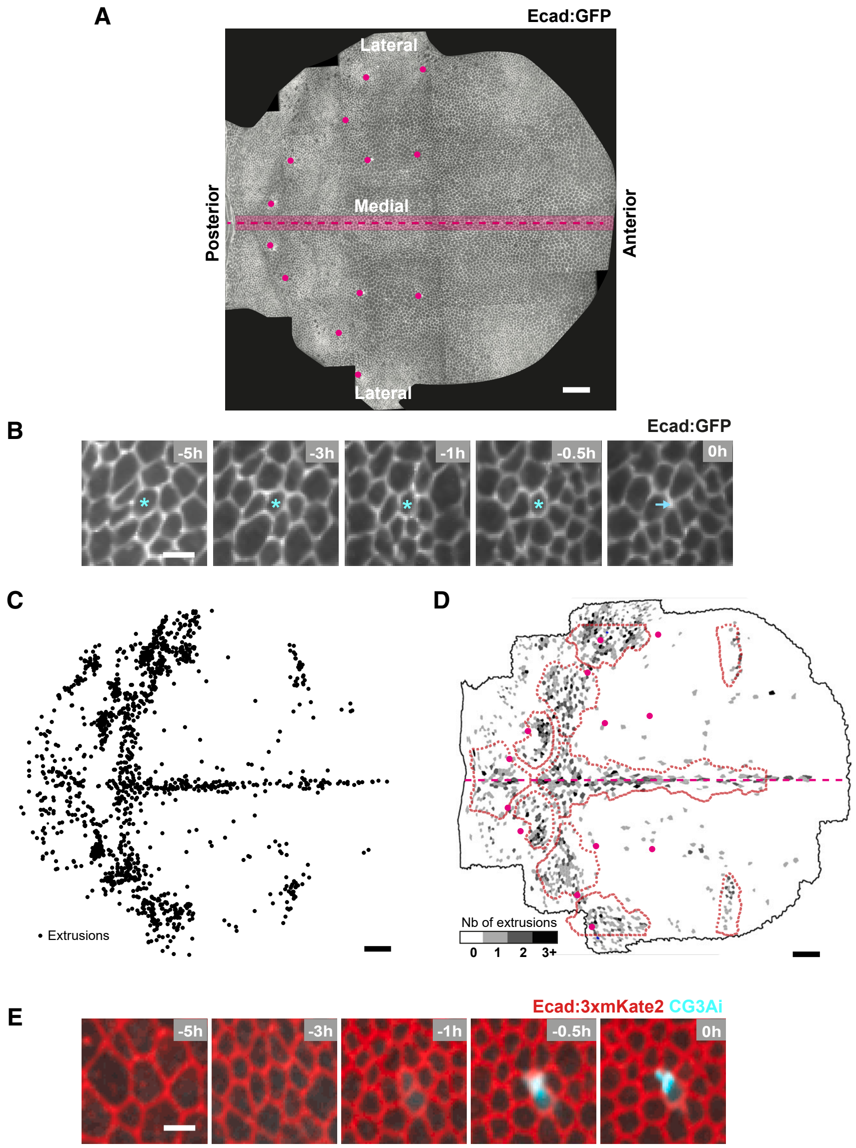

Figure 1. Spatiotemporal patterns of apoptosis in the *Drosophila* notum

(A) Pupal notum labeled by Ecad:GFP at 20 hAPF. Magenta dashed line: a-p axis. Magenta shaded domain: a 3-to-4-cell-wide stripe of large and elongated cells forming the midline previously shown to be highly apoptotic. Magenta dots: macrochaetae.

(B) Time-lapse images of Ecad:GFP showing an extruding cell (cyan asterisk). Time (h) is set to 0 at apical extrusion marked by the loss of cell apex (cyan arrow).

(C) Spatial map of cell extrusions in the notum. Black dots indicate the positions where extrusions occurred between 15 and 32 hAPF.

(D) Extrusions shown on a segmented image of the notum shown in (A) at 13 hAPF, where cells are color coded according to the number of upcoming extrusions a cell or its progeny will undergo until 32 hAPF (white: no extrusion, black: at least 3 extrusions). Thick dashed red lines: apoptosis mask corresponding to regions with higher apoptotic density between 15 and 30 hAPF. Magenta dashed line: a-p axis. Magenta dots: macrochaetae.

(E) Time-lapse images of Ecad:3xmKate2 and the GC3Ai caspase fluorescence reporter prior to and during cell extrusion. Time (h) is set to 0 at apical extrusion.

Scale bars: 50 μm (A, C, and D), 5 μm (B and E).

See also Figure S1, Videos S1 and S2, and Table S2.

morphogenetic movements associated with proliferation and apoptosis from 14 hAPF onward.[31,32,39–41] As such, it has provided a valuable model to explore the conserved links between biochemical and mechanical factors contributing to cell and tissue dynamics.[31–33,40,42–48] Here, by combining the time-lapse imaging of the developing notum with the tracking of tens of thousands of cells during up to 20 h of development, we characterized the spatiotemporal pattern of apoptosis in this tissue. By quantitatively analyzing the lifelong behavior of future apoptotic cells prior to caspase activation, we found that long before their extrusion, these cells are characterized by two key geometric features: a small apical area compared with other cells in the tissue and a small relative apical area compared with the immediate neighbors. These distinct features are sufficient to recapitulate the tissue-scale apoptotic pattern. We then studied each of these size features and identified two molecular pathways involved in their respective regulation. Collectively, our work establishes a tight link between two geometric features and apoptosis in developing epithelium.

RESULTS

Characterization of the spatiotemporal pattern of apoptosis in the *Drosophila* notum

Past studies of apoptosis in the monolayered *Drosophila* notum often analyzed a specific and highly apoptotic region of the tissue, the midline, a 3-to-4-cell-wide stripe of large and elongated cells along the anterior-posterior (a-p) tissue axis[31–33] (Figure 1A). Unlike what happens in the other notum regions, caspases are activated in midline cells prior to any morphogenetic movements of the pupal notum.[47,48] To investigate the factors controlling life and death decisions at the tissue scale, we first further characterize whether apoptosis is patterned in other regions of the tissue. We performed time-lapse imaging of the developing notum using the *adherens* junction marker Ecadherin:GFP (Ecad:GFP) from 15 hAPF onward (Figure 1A). Upon the segmentation of these movies, we used previously implemented befitting tools that give us access to large datasets of several tens of thousands of cell positions, apical geometry, and behaviors, as well as their contribution to morphogenesis.[39] These tools allow us to track various cell processes, such as cell division, which is known to be strongly patterned in space and time in the notum.[39,40] In addition, we can track and analyze cell extrusions (Figure 1B), which often concur with apoptosis in epithelial tissues.[2,49] We mapped extrusions in the whole pupal tissue between 15 and 32 hAPF, corresponding to the tracking of about 23,700 ± 3,000 cells per heminotum over time (N = 5 heminota,

Please cite this article in press as: Cachoux et al., Epithelial apoptotic pattern emerges from global and local regulation by cell apical area, Current Biology (2023), https://doi.org/10.1016/j.cub.2023.09.049

Figures 1C and 1D; Video S1). We found that about 850 ± 180 extrusions occur per heminotum. Notably and extending our previous observations,[39] these extrusions are spatially patterned across the tissue, with some regions displaying a high number of extruding cells and others displaying nearly no cell extrusion during this time range (Figures 1C and 1D). Using spatial landmarks on the notum (namely several macrochaetae and the midline) to register multiple nota from different animals, we verified that the spatial distribution of extrusion is comparable among animals (Figure S1B). It is also remarkably symmetric with respect to the midline (Figures 1C and 1D). Moreover, the temporal distribution of extrusions is also similar among animals (Figures S1C and S1D).

Extruding cells can be either alive, which does not rule out their later death, or in the process of undergoing apoptosis through caspase activation.[2,21,49] To distinguish between these two cases, we performed time-lapse imaging with the Ecad:3xmKate2 marker and GC3Ai, a live caspase-activated fluorescent reporter[50] (Figure 1E). Across the entire notum, the visual inspection of extruding cells revealed that a burst of caspase activity precedes extrusion (n = 96 out of 100 cells in N = 3 nota) (Figure 1E; Video S2). Using His2B:RFP, we also verified that extruded cells show chromatin condensation, indicative of apoptosis (n = 65 out of 65 cells; Figure S1E). In *Drosophila*, apoptosis is controlled by the expression of the *rpr*, *hid*, and *grim* pro-apoptotic genes that act upstream of the inhibitor of apoptosis proteins, IAP (Diap in *Drosophila*), and of caspase activation.[9] We found that inhibiting *rpr*, *hid*, and *grim* functions by RNAi (RHG^{RNAi})[51] led to a drastic reduction in extrusions within the tissue (11 ± 5 extrusions per heminotum; N = 6). Together, these data argue that the study of cell extrusions in the notum informs us of the characteristics of apoptotic cells. Overall, these quantitative characterizations raise the questions of how the apoptotic regions are determined and how some cells die but other cells remain within these regions.

Tissue contraction does not correlate with notum apoptotic pattern

Recent studies have linked tissue compression to the extrusion of wild-type (WT) cells in a variety of systems, such as cell cultures, developing zebrafish epidermis, and around tumor cells in the *Drosophila* notum.[31–35] These studies raise the question of whether endogenous tissue contraction can account for a tissue-scale pattern of apoptosis. During pupa metamorphosis, the notum undergoes tissue deformations that can be characterized as a combination of isotropic contraction-expansion and anisotropic convergence-extension and that substantially vary over space and time.[39] To explore whether the apoptotic pattern in the notum could stem from isotropic contraction, we studied the relative timing of apoptosis and mesoscopic tissue contraction in various regions of the notum. Apoptosis being spatially patterned at the tissue scale with some regions harboring a high number of apoptoses, we first created an archetypal mask of apoptotic regions using the data from 5 heminota (Figure 1D). This archetypal mask contains 77% ± 8.8% (N = 5) of all apoptoses occurring between 15 and 30 hAPF. We could, therefore, define archetypal apoptotic regions characterized by a high apoptotic rate, whereas others are nearly devoid of extrusion. On segmented Ecad:GFP time-lapse movies, we then tracked patches of cells corresponding to regions within the apoptotic mask as well as regions outside of the mask to quantify their respective areas over time (Figures 2A and S1F). A decreasing patch area corresponds to patch contraction, whereas a patch with an increasing area indicates expansion. We found a wide variety of behaviors in the notum: although posterior lateral regions exhibit tissue contraction followed by cell apoptosis (regions 3 and 4, Figure 2B), other regions such as the central lateral zone exhibit contractions of similar magnitude without subsequent cell death (region 6, Figure 2B). Moreover, apoptosis sometimes precedes tissue contraction, as seen in the midline (regions 1 and 2, Figure 2B). Overall, tissue contraction does not always precede or induce apoptosis. This suggests that tissue physiological contraction by itself cannot explain the apoptotic pattern observed at the scale of the whole tissue.

Early cell geometric features characterize future apoptotic cells

Cell apical area can be directly and substantially impacted by mechanical tissue contraction or expansion. Thus, studies linking tissue contraction to cell apoptosis may indirectly connect apical size decrease to apoptosis. In addition, seminal work in individual cells in culture has linked cell fate and cell spreading.[52–55] We, therefore, hypothesized that the apical size of cells could play a role in the control of physiological apoptosis in the developing notum. The notum stands as an excellent system to test this hypothesis, as its epithelial cells are characterized by a large variety of cell sizes at 13 hAPF (Figure 3A, left). Moreover, this initial difference in cell size does not stem from distinct cell-cycle phases since 12 hAPF notum cells are all in the G2 phase of the cell cycle prior to undergoing successive waves of division.[38,56–58] Importantly, the last hour of life of apoptotic cells is characterized by a drastic and rapid decrease of the cell apex, ultimately leading to extrusion.[19] Therefore, to identify possible pre-determining geometric factors of apoptosis, we decided to study the apical size of future apoptotic cells throughout their lives prior to this last hour. Hereinafter, we will refer to this phase as the "pre-extrusion" phase of cell lives, that is, the phase before cells exhibit any major known morphological sign of apoptosis.[19]

To do so, we quantified the apical area of apoptotic and non-apoptotic cells throughout their lives on segmented Ecad:GFP movies. The average area of the future apoptotic cells was measured by averaging their area throughout their lifespan up to 1 h prior to their extrusion (pre-extrusion phase); for control, the apical areas of all non-apoptotic cells of the tissue were averaged at the same time points as the apoptotic cells. We found that the average areas of future apoptotic cells are 38% smaller than the average notum cell area (Figure 3B). Moreover, the area distribution of apoptotic cells is more skewed toward small sizes. This suggests that cells with small apical areas are more likely to undergo apoptosis. We, therefore, quantified the probability of a cell to die as a function of its area, and accordingly, we found that the probability of becoming apoptotic sharply increases with decreasing area (Figure 3C). Furthermore, by averaging the cell area of future apoptotic cells, we found that area is rather steady prior to the rapid extrusion phase, as cell area only decreased by 11% starting 5 h prior to delamination (Figure S2A). Since caspase activation can be observed to increase 3 h prior to cell

Please cite this article in press as: Cachoux et al., Epithelial apoptotic pattern emerges from global and local regulation by cell apical area, Current Biology (2023), https://doi.org/10.1016/j.cub.2023.09.049

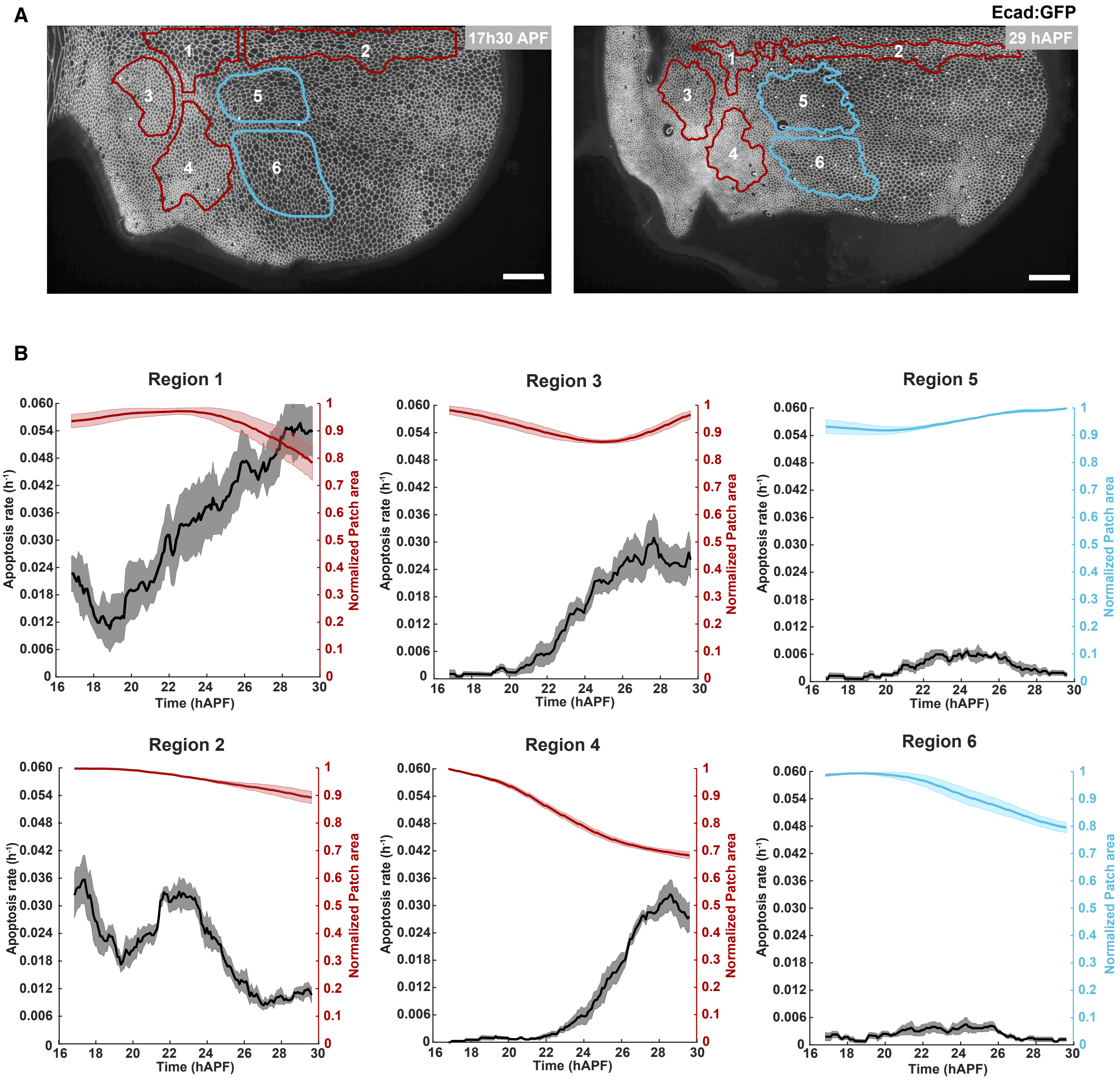

Figure 2. Relative timings of tissue contraction and apoptosis in different regions of the notum

(A) Time-lapse images of an Ecad:GFP notum at 17h30 APF and 29 hAPF. Thick lines indicate six regions in the tissue that were tracked over time, four regions of the apoptotic mask (red, regions # 1–4) and two regions outside of the apoptotic mask (cyan, regions # 5 and 6).

(B) Graph of the temporal evolution of the rate of apoptosis (black, mean ± SEM) and the region surface area, normalized to its maximum value (color coded as for the corresponding regions, mean ± SEM), in each of the six regions indicated in (A). A decrease in the region area (such as that in region 2), therefore, indicates contraction, whereas an increase (such as that in region 5) indicates expansion. N = 4 heminota.

Scale bars: 50 μm.

See also Figure S1 and Table S2.

extrusion (Figure S2B), we also verified that the apical areas of future apoptotic cells are significantly smaller than the average notum cell area prior to caspase activation by removing the last 3 h of their lives from their time average (Figure S2C). Overall, during their pre-extrusion phase, future apoptotic cells are characterized by a smaller apical area that modestly decreases over time and that precedes the rapid and drastic apical shrinkage associated with cell extrusion.

To test whether the observed smaller apices could be a consequence of apoptotic signaling, we inhibited apoptosis by performing a simultaneous local inhibition of the *rpr*, *hid*, and *grim* genes, which act upstream of caspase, through the clonal

Please cite this article in press as: Cachoux et al., Epithelial apoptotic pattern emerges from global and local regulation by cell apical area, Current Biology (2023), https://doi.org/10.1016/j.cub.2023.09.049

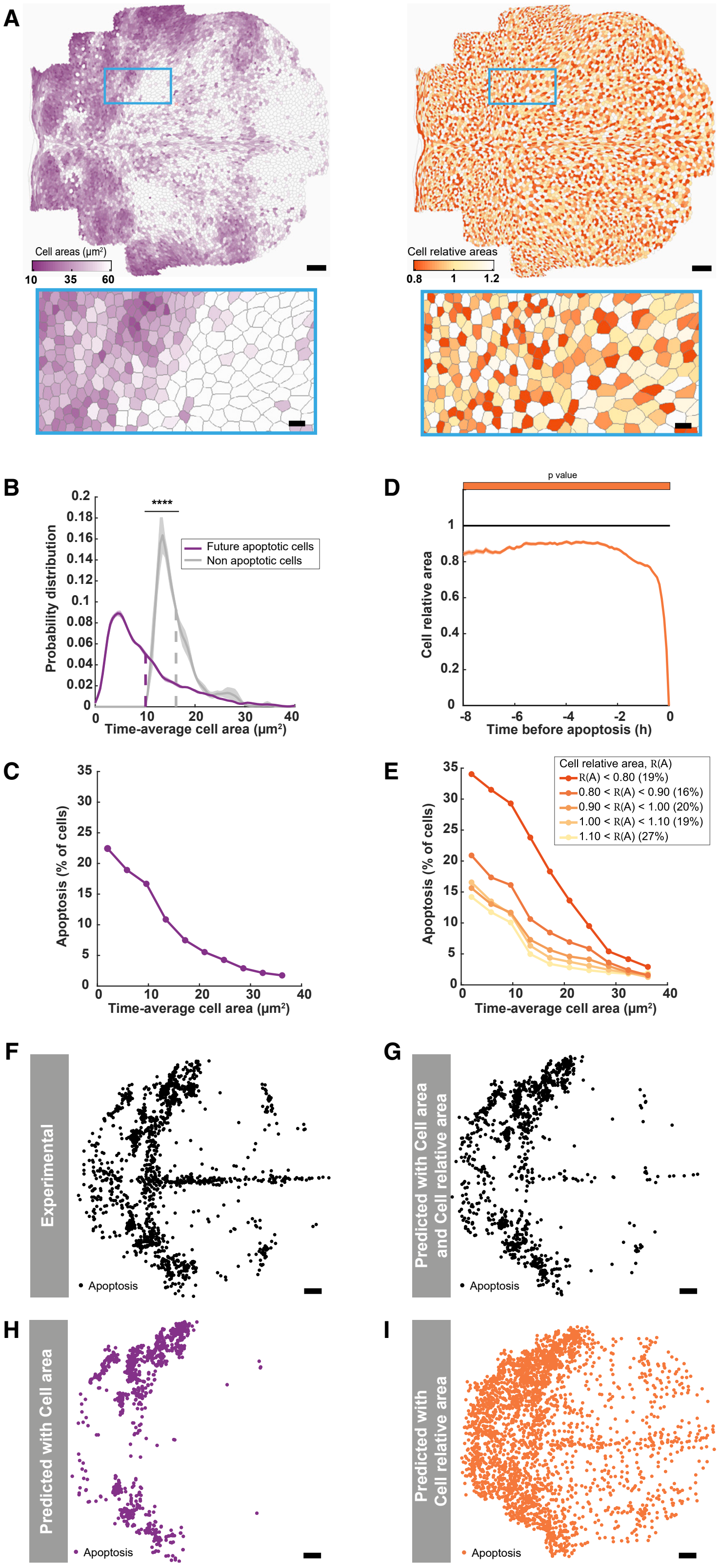

Figure 3. Future apoptotic cells display early and predictive geometric features

(A) Segmented images of the notum shown in Figure 1A at 13 hAPF (top) and close-up of the region outlined in blue (bottom) where cells are color coded according to their apical areas (left) and relative areas (right).

(B) Distributions of the apical areas of future apoptotic cells averaged over their pre-extrusion phase (purple, mean ± SEM) and of the apical areas of all cells of the tissue taken at similar time points as the apoptotic cells (gray, mean ± SEM). Curves are smoothed over 3 data points. The area below each curve is one. n = 4,244 cells from N = 4 heminota. Dashed lines: average values. Future apoptotic cells are on average 38% smaller than non-apoptotic cells, $p = 3.1 \times 10^{-98}$, Student's t test.

(C) Graph of the percentage of cells undergoing apoptosis versus cell apical areas. Cells whose fate is known are binned depending on their apical areas averaged over their pre-extrusion phase, and the ratio of apoptotic cells by the total number of cells is computed in each bin. The curve is smoothed over 3 points. n = 32,638 cells from N = 4 heminota.

(D) Graph of the mean relative apical area of apoptotic cells (orange, mean ± SEM) versus time before their apical extrusion. Time-evolution curves of single-cell relative areas have been aligned to their respective times of apical extrusion set to t = 0. n = 4,465 cells from N = 4 heminota. Horizontal bar: p values of Student's t tests comparing the relative area with an average value of 1 every 15 min, color coded according to the p value (dark orange $p < 0.01$).

(E) Graph of the percentage of cells undergoing apoptosis versus cell apical areas (same data as in C) broken down into a family of curves, one curve for each bin of cell relative apical areas. The percentage of cells in each bin is indicated. n = 32,638 cells from N = 4 heminota.

(F) Experimental spatial map of apoptosis in the notum (as in Figure 1C).

(G–I) Predicted spatial maps of apoptosis using both the cell area and relative apical area (G, black dots, F1-score = 0.55), the cell areas only (H, purple dots, F1-score = 0.48), and the cell relative areas only (I, orange dots, F1-score = 0.38). F1-score for a random model is equal to 0.14.

Scale bars: 50 µm (A, top, and F–I), 10 µm (A, bottom). ****p<0.0001.

See also Figure S2 and Tables S1 and S2.

Please cite this article in press as: Cachoux et al., Epithelial apoptotic pattern emerges from global and local regulation by cell apical area, Current Biology (2023), https://doi.org/10.1016/j.cub.2023.09.049

expression of the RHG^{RNAi} in Ecad:GFP tissues. To compare apical cell size in RHG^{RNAi} and control cells, despite the substantial cell size heterogeneity in the notum, we measured the apical area of cells in RHG^{RNAi} clones and compared them with that of the corresponding control cells located symmetrically with respect to the midline in the same animal (Figure S2D, left). We found that inhibiting the *RHG* genes has only a very mild effect on cell apical area throughout tissue development, with the average size of RHG^{RNAi} cells being bigger than that of control cells by 1.9 μm^2 at most, corresponding to a modest increase of 8% during short periods of time (Figure S2D, right). Since future apoptotic cells are characterized by an average area 38% smaller than that of non-apoptotic cells during their pre-extrusion phase (Figure 3B), the small apical area of future apoptotic cells could be a predictive factor of apoptosis rather than a consequence of the expression of the *RHG* genes.

The notum displays several regions within which cell area is locally quite homogeneous (Figure 3A, left). Therefore, in the hypothesis of a regulation of cell death by apical area only, entire regions of small cells could be primed to commit apoptosis, thereby potentially jeopardizing tissue integrity. Yet, apoptosis remains a relatively rare event. We thus decided to investigate how, among small cells, some are eliminated via apoptosis, whereas some other cells are not. We, therefore, looked for additional features that could help distinguish a future apoptotic cell within its local environment. To do so, we investigated the role of the relative apical area between a future apoptotic cell and its immediate neighbors. We defined the relative area as $\mathcal{R}(A) = A_i/\langle A_j \rangle$, namely the apical area of a cell i divided by the average area of its direct neighbors j, a dimensionless metric such that $\mathcal{R}(A) < 1$ if a cell apex is smaller than the average apex of its neighbors (Figure 3A, right). Thus, if a future apoptotic cell has the same apical size as its neighbors during its pre-extrusion phase, one expects $\mathcal{R}(A) \approx 1$, which is what we observed for non-apoptotic cells in apoptotic regions (Figure S2E). Strikingly, we found that, on average, future apoptotic cells are instead characterized by $\mathcal{R}(A) = 0.87 \pm 0.03$ (mean ± SEM) during their pre-extrusion phase, indicating that their apical area is 13% smaller than the average area of their neighbors (Figure 3D). Notably, on average, apoptotic cells are smaller than their neighbors several hours before the extrusion phase and caspase activation (Figures 3D and S2B). We, therefore, conclude that future apoptotic cells are characterized by two early distinctive features: a small area with respect to cells in the tissue and a small relative area with respect to the immediate neighbors of the apoptotic cells.

Combination of area and relative area predicts the apoptotic pattern

To better understand the role of geometric factors in the determination of cell death, we then explored the respective contributions of the apical area and relative apical area to apoptosis. Importantly, given the ordered patterning of cell size in the tissue and the existence of large regions of cells with similar sizes, we found that the area and relative area are poorly correlated, as illustrated by the maps of cell area and cell relative area that display completely different patterns (Figures 3A and S2F). This suggests that each quantity could carry different information and play different roles at the cell level. To evaluate the relative impacts of these two apical parameters on apoptosis, we used a multivariate logistic regression (Table S1) that models the probability to die as a function of these factors. Importantly, we found that both the area and relative area are associated with significant non-zero coefficients, which represent their impact on the probability of apoptosis when the other variable is held constant. Thus, the two parameters independently correlate with the probability of apoptosis, thereby arguing for distinct roles. This is confirmed when plotting the variation of the probability to undergo apoptosis as a function of both parameters (Figure 3E): it shows that “for a given apical size,” the cells that are surrounded by neighbors with bigger apices have a higher probability to die than cells that are surrounded by neighbors of similar or smaller size. Overall, the two distinct cell features we identified, cell apical area and relative area, both correlate with the probability of a cell to undergo apoptosis.

Are these features predictive of the spatial pattern of apoptosis? To answer this question, we developed a prediction model trained on experimental data. The training and validation datasets consisted of the cells from 6 developing heminota, whereas the test dataset contained the cells from 3 other developing heminota. For each cell, the area and relative area (averaged over the pre-extrusion phase), as well as fate, were extracted. These data were then used to train an adapted k-means clustering algorithm, which was compared with other types of models (see details in STAR Methods). We verified that our best predictive model recapitulates the majority of the apoptotic pattern in the notum (Figures 3F, 3G, S2G, and S2H). Interestingly, we found that both the area and relative area are needed to successfully predict the apoptotic pattern, as predictions using only one of these two features were less accurate (Figures 3H, 3I, S2I, and S2J). Moreover, only few apoptoses are predicted in the highly apoptotic anterior midline (Figure S2K). Since midline cells are characterized by their larger apices and the specific expression of apoptotic factors very early in development,[48] our finding that the expression of the *RHG* genes is not a determinant of the area of future apoptotic cells is strengthened (Figure S2D). Together, our results indicate that the two distinct and early size features, namely a small apical area and a small relative apical area, are predictive of a future apoptotic fate.

Reduction of cell apical area by cell division is required for subsequent apoptosis

We next investigated whether apoptosis is controlled by the first of these two parameters, the apical area. Cell division and growth are major regulators of cell size. In the pupal notum, apical cell growth is relatively minor during the cell cycle (Figure S3A). Consequently, if taken at the same point in their cell cycle, the average cell apical area substantially decreases by 49% ± 0.5% with each division round (Figure S3A; Video S3). Importantly, we verified that at birth the apical areas of future apoptotic cells are already significantly smaller than the average notum cell area (Figure S3B).

We, therefore, decided to study the interplay between cell division and apoptosis to test whether cell area can directly modulate cell apoptosis. First, comparing the spatial patterns of apoptosis and divisions revealed that apoptosis is sparse in regions where cells divide only once during pupal development;

Please cite this article in press as: Cachoux et al., Epithelial apoptotic pattern emerges from global and local regulation by cell apical area, Current Biology (2023), https://doi.org/10.1016/j.cub.2023.09.049

more specifically, 75% of the regions of apoptosis overlap with regions where cells divide 2 times or more (Figures 4A and 4B; Video S4). Second, we compared the global timings of both cell processes and found that apoptosis substantially increases after the first wave of divisions (Figure 4C). Accordingly, we observed that 88% ± 4.0% (N = 4 heminota) of the apoptotic cells originated from a dividing cell; this percentage reaches 96% ± 2.6%, if midline cells are excluded. Third, after each division round, we characterized the fate and area of the daughter cells (Figures S3A and S3C). We found that the more a cell has divided, and thus the smaller its apex, the higher its probability to undergo apoptosis instead of entering another division (Figure 4D). These results suggest that cell division promotes subsequent apoptosis.

Since at 12 hAPF pupal cells are blocked in G2, we explored the role of cell division by blocking epithelial divisions with the overexpression of *tribbles* (*trbl*^{OE}), an inhibitor of the G2/M transition of the cell cycle[59–61] (Figures 4E and 4I). Decreasing the division number by *trbl* overexpression and thus preventing cells from halving their size led to the almost complete disappearance of apoptosis. The average apoptosis rate, measured as the number of apoptoses divided by the initial number of cells, falls to 1.5% ± 0.6% versus 19% ± 2.7% in control notum (Figures 4F and 4J). Alternatively, we increased proliferation to further reduce cell apical area by overexpressing *CyclinE* (*CycE*^{OE}), a regulator of the G1/S transition[62] (Figures 4G and 4I). *CycE* overexpression almost triples the occurrence of cell extrusion, as the average extrusion rate increases to 63% ± 15% (Figures 4H and 4J). As observed in control condition, most of the extruding cells exhibited an accumulation of the apoptotic GC3Ai marker upon *CycE* overexpression (Figure S3D). Strikingly, this increase in programmed cell death is global and affects the entire notum, including the usually non-apoptotic regions of the tissue (Figure 4H). Notably, our predictive model, trained on the apical area and the apoptosis of WT tissues, predicts both a global increase in apoptosis in *CycE*^{OE} tissues and a drastic reduction in apoptosis in *trbl*^{OE} tissues (Figure S3E). Altogether, we conclude that, by substantially reducing cell apical area at each division round, cell division modulates apoptosis.

Cell apical area modulates apoptosis

To further test the impact of cell apical area on apoptosis, we focused thereafter on the posterior central region of the notum where a substantial part of apoptoses occurs, thus facilitating the analysis of the contribution of apical cell size to apoptosis control. To modulate cell apical area, we used stretchable polydimethylsiloxane (PDMS) membranes to exert uniaxial compaction by around 15% along the medio-lateral axis on developing nota (Figures 5A and S4A; see STAR Methods for details). The compaction was gradually applied within 30 min, after which we studied subsequent tissue dynamics during development. In this region, as measured through the segmentation and automated quantification of cell areas prior to and after 30 min of compaction, we found that cells after compaction had, on average, an apical area 19% smaller than that of non-compacted tissues while having a relative area similar to that of non-compacted tissue cells (Figures 5B, 5C, and S4B). If cell apical area is, indeed, a direct determinant of cell apoptosis, we should be able to predict an increase in cell apoptosis based on the compaction-induced variation of cell size. Our predictive model, applied to the apical size pattern of non-compacted animals, allowed us to estimate that a 19% area change would be associated with an increase in the rate of apoptosis by 24% ± 3% (Figure 5D). Furthermore, despite the rather spatially homogeneous apical size reduction induced by the PDMS compaction, we also predicted that this apoptosis rate increase would not be spatially homogeneous. Indeed, the additional apoptoses that are predicted to be induced by compaction were spatially biased toward apoptotic regions, with 69% ± 6.0% of the extra apoptoses predicted to occur within the apoptotic mask (which represents 48% of the total region analyzed) (Figures 5E and S4C). Experimentally, we observed that compacted pupae show a 22% higher extrusion rate than non-compacted ones, in good accordance with the increase that we predicted (Figures 5D and S4D). In both non-compacted and compacted conditions, the percentages of extruding cells accumulating the GC3Ai apoptotic marker were similar, confirming that the additional extrusions are associated with apoptosis (Figure S4E). Moreover, the spatial distribution of apoptosis is not significantly changed by compaction, with 81% ± 1.8% of apoptoses occurring in the apoptotic mask in compacted pupae versus 88% ± 4.6% in control ones (Figure 5F). These results confirm that tissue compaction alone is not the main regulator of apoptosis, since a nearly homogeneous tissue-scale reduction in cell apical sizes drives a heterogeneous increase in apoptosis, substantially biased toward regions of smaller cells. To further confirm that cell apical area rather than compaction itself promotes apoptosis, we also explored the correlation between the magnitude of compaction and death. We found that, although apically larger cells get more compacted than the smaller ones upon tissue compaction (Figure 5G), smaller cells still tend to die more than the larger ones (Figure 5H). Taking our results together, we propose that the cell apical area is a determinant of the probability for a cell to undergo apoptosis and, consequently, a relevant parameter in the shaping of the global apoptotic pattern in the tissue.

Linking cell apical area, cell death, and Hippo/YAP pathway activity

Having identified the apical area as a regulator of apoptosis, we then aimed at characterizing the signaling pathways contributing to this regulation. The MAPK/ERK (Mitogen-Activated Protein Kinase/Extracellular signal-Regulated Kinase) pathway is known to regulate apoptosis via the transcriptional regulation of the pro-apoptotic gene *hid*.[33,63,64] Furthermore, ERK signaling is involved in cell death associated with genetically induced cell crowding.[32,33] We thus hypothesized that the MAPK/ERK pathway could be involved in regulating cell death as a function of apical area. ERK-KTR:GFP reporters have been previously described to quantify ERK activity.[65,66] We developed an ERK-KTR:GFP reporter expressed under an ubiquitin promoter and validated the use of this reporter to quantify ERK activity in *Drosophila*, measured as the ratio between cytoplasmic and nuclear GFP fluorescence (Figures S5A–S5D). However, we found that ERK activity does not correlate with cell apical area (Figure S5E).

We then investigated the Hippo/YAP (Yorkie, Yki in *Drosophila*) pathway, which is involved in mechanosensing,[67] in cell proliferation,[68] and in the modulation of apoptosis via the transcriptional

Please cite this article in press as: Cachoux et al., Epithelial apoptotic pattern emerges from global and local regulation by cell apical area, Current Biology (2023), https://doi.org/10.1016/j.cub.2023.09.049

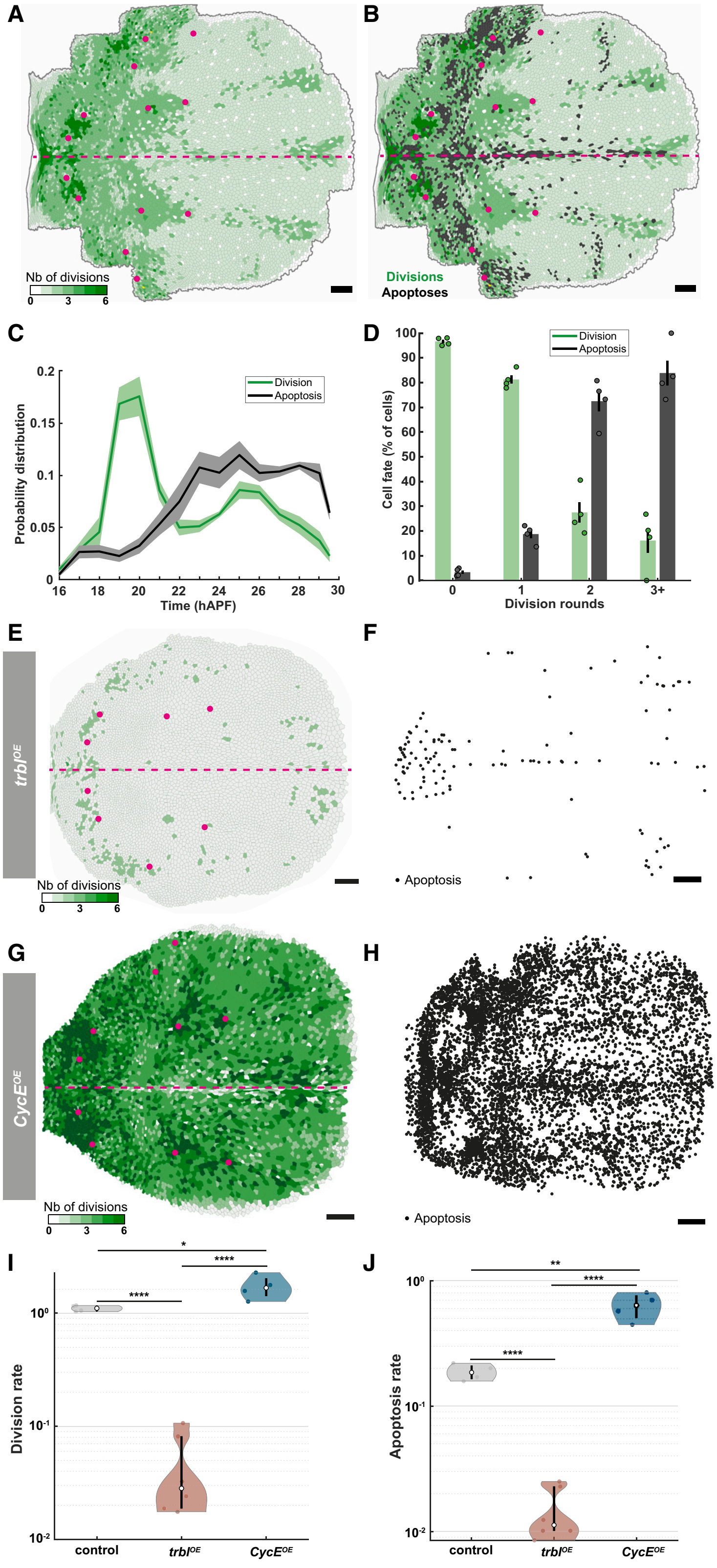

Figure 4. Coupling between proliferation and apoptosis

(A) Divisions shown on a segmented image of the notum shown in Figure 1A at 13 hAPF. Cells are color coded depending on the upcoming number of divisions a cell and its progeny will undergo during development. Darker shades of green indicate more divisions. Magenta dashed line: antero-posterior axis. Magenta dots: macrochaetae.

(B) Divisions shown on a segmented image of the notum shown in Figure 1A overlapped with the binarized extrusion map of Figure 1D (black, cells whose progeny or themselves will undergo apoptosis). Magenta dashed line: a-p axis. Magenta dots: macrochaetae.

(C) Distribution of divisions (green, n = 26,728) and apoptoses (black, n = 4,468) over developmental time. The area under each curve is set to one. N = 4 heminota.

(D) Graph of the proportion of cells between 15 and 30 hAPF undergoing either division (green, n = 26,728) or apoptosis (dark gray, n = 4,468), depending on the division rounds they originate from. Dots: individual heminota, N = 4.

(E) Divisions shown on a segmented *trbl*^{OE} notum at 15 hAPF. Cells are color coded depending on the upcoming number of divisions a cell and its progeny will undergo during development. Darker shades of green indicate more divisions. Magenta dashed line: a-p axis. Magenta dots: macrochaetae.

(F) Spatial map of apoptosis in the *trbl*^{OE} notum shown in E. Dots indicate the locations where apoptoses occurred between 16 and 29 hAPF.

(G) Divisions shown on a segmented *CycE*^{OE} notum at 15 hAPF. Cells are color coded depending on the upcoming number of divisions a cell and its progeny will undergo during development. Darker shades of green indicate more divisions. Magenta dashed line: a-p axis. Magenta dots: macrochaetae.

(H) Spatial map of apoptosis in the *CycE*^{OE} notum shown in (G). Dots indicate the locations where apoptoses occurred between 16 and 29 hAPF.

(I) Plot of the division rates in control (gray, N = 4 heminota), *trbl*^{OE} (brown, N = 6 heminota), and *CycE*^{OE} (blue, N = 4 heminota) notum between 16 and 29 hAPF. Log-scale. The division rate is the number of divisions divided by the initial number of cells. White dot: average, thick black line: first to third quartiles, dots: individual heminota. p values: $p = 9.5 \times 10^{-3}$ (control versus *trbl*^{OE}), p = 0.029 (control vs. *CycE*^{OE}), $p = 9.5 \times 10^{-3}$ (*CycE*^{OE} versus *trbl*^{OE}), Mann-Whitney U test.

(J) Plot of the apoptosis rates in control (gray, N = 4 heminota), *trbl*^{OE} (brown, N = 6 heminota), and *CycE*^{OE} (blue, N = 4 heminota) notum between 16 and 29 hAPF. Log-scale. Apoptosis rate is the number of apoptoses divided by the initial number of cells. White dot: average, thick black line: first to third quartiles, dots: individual heminota. p values: $p = 9.5 \times 10^{-3}$ (control versus *trbl*^{OE}), p = 0.029 (control vs. *CycE*^{OE}), $p = 9.5 \times 10^{-3}$ (*CycE*^{OE} versus *trbl*^{OE}), Mann-Whitney U test.

Scale bars: 50 μm. $^{*}p<0.05$; $^{**}p<0.01$; $^{****}p<0.0001$.

See also Figure S3, Videos S3 and S4, and Table S2.

Please cite this article in press as: Cachoux et al., Epithelial apoptotic pattern emerges from global and local regulation by cell apical area, Current Biology (2023), https://doi.org/10.1016/j.cub.2023.09.049

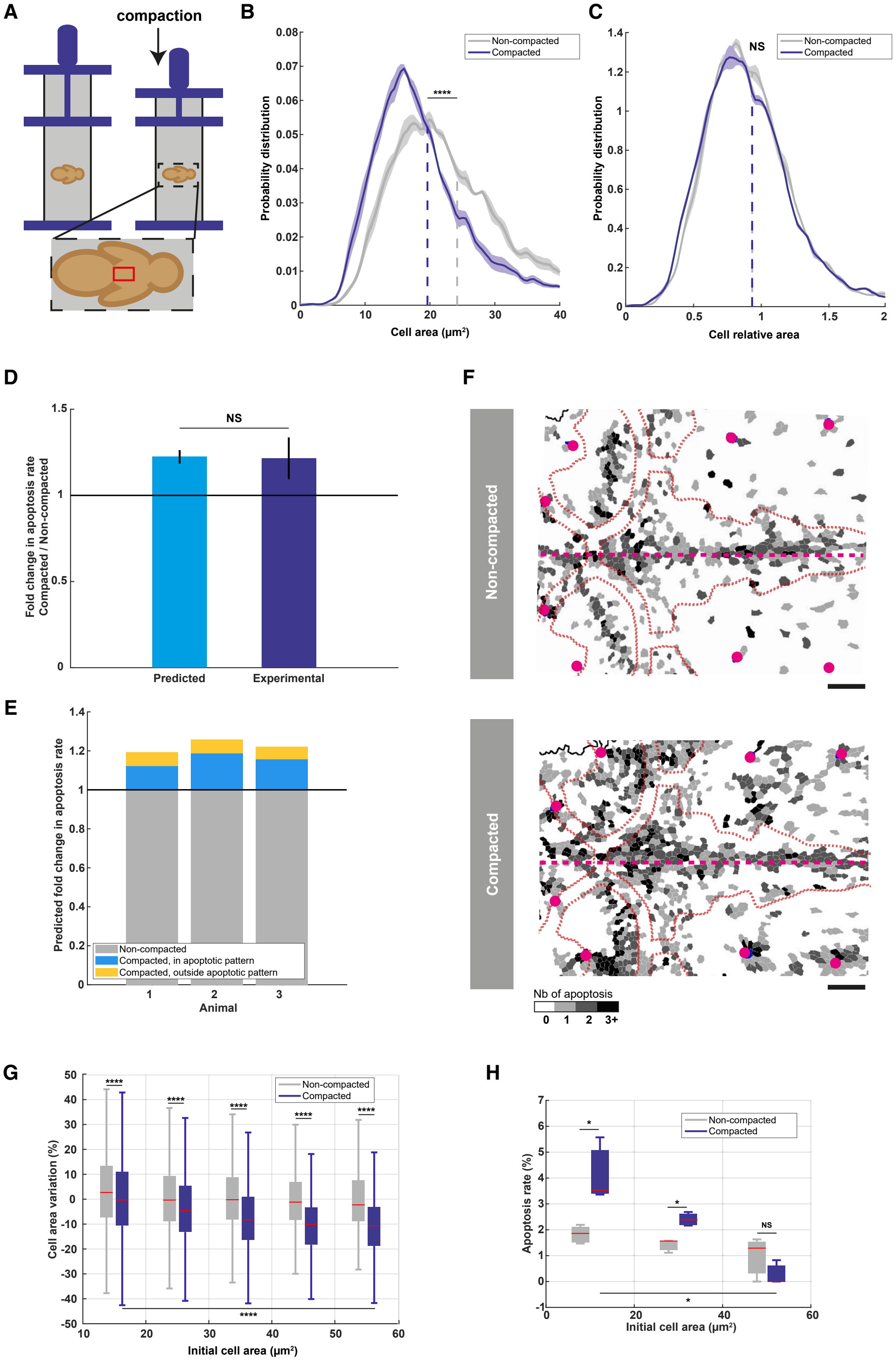

Figure 5. Uniaxial mechanical compaction changes the apoptosis rate.

(A) Schematic representation of the experimental setup. Between 15h30 and 16h30 APF, Ecad:3xGFP pupa without pupal case (brown) were glued on a 150% pre-stretched PDMS stripe (gray) attached to a custom-made compression device (dark blue). In compacted pupae, the pre-stretched PDMS was progressively

(legend continued on next page)

control of the expression of the apoptosis inhibitor *Diap1*[68–71] and of the microRNA *bantam (ban)*.[72] The expressions of the *Diap1* or *ban* genes can be used as readouts of the Hippo/YAP signaling pathway activity, and they are measured using two distinct transgenes: *Diap1-nls:GFP*[73] and *ban-nls:GFP*,[74] which express *nls-GFP* under the control of the *Diap1* and *ban* promoters, respectively. Unlike ERK, Hippo/YAP activity scales with apical cell size[43]: we recently showed that the intensity of *ban-nls:GFP* and of *Diap1-nls:GFP* positively correlates with cell apical area in the central posterior region of the notum[43] (Figures 6A, S5F, and S5G). Moreover, we found that PDMS-mediated tissue compaction led to decreased *ban-nls:GFP* levels (Figure S4F). This finding suggests that the Hippo/YAP signaling pathway can be diminished by the reduction in cell apical area induced by tissue compaction. We then sought to test whether impacting Hippo/YAP activity could disturb the relationship between cell apoptosis and apical size. Ajuba (Jub) is a regulator of Hippo signaling, whose clustering with the Warts kinase upregulates Yki activity.[43,75–77] We, therefore, quantified the amount of Jub clustering in cells and found that future apoptotic cells are characterized by a lower clustering of Jub than their non-apoptotic surrounding cells (Figure 6B), thereby suggesting a lower Yki activity in future apoptotic cells. In addition, we locally inhibited Yki activity by the clonal expression of *jub*^{RNAi} during pupal development in the central posterior notum and used the non-clonal symmetric contralateral regions as control (Figure 6C). We found that *jub* knockdown enhances apoptosis, as revealed by the quantification of the number of extruding cells and the accumulation of the GC3Ai marker (Figure S5H). Importantly, this effect is not homogeneous but instead increases with cell apical area (Figure 6D). This is consistent with a model in which the higher Yki activity in large cells would block their apoptosis. Since the scaling between Hippo/YAP activity and apical cell size is mediated by the α-Actinin (*Actn*) that promotes Jub clustering,[43] we then further tested the role of this scaling by compromising it by locally reducing Actn function in the posterior central notum. We found that, at a given apical area, apoptosis is also enhanced in *Actn*^{RNAi} cells; once again, as in *jub*^{RNAi} clones, the fold change in apoptosis rate increases with cell apical size (Figure 6E). Overall, our results indicate that a low Yki activity, as found in small WT cells, is associated with an increased probability to undergo apoptosis. Preventing the scaling between Hippo/YAP activity and apical size by inhibiting *Actn*[43] impacts the modulation of cell survival by cell apical area. Together, we conclude that the scaling between cell apical size and Hippo/YAP signaling can account for the control of apoptosis by apical size.

Cell *relative* apical area can impact local apoptosis

Next, we studied the role of cell relative apical area, which is the second size-related feature of apoptotic cells that is predictive of epithelial apoptosis. To test whether modulating relative cell size changes the apoptosis rate, we sought to induce relative size heterogeneity in otherwise genetically identical cells. Given that the Target of Rapamycin (Tor) protein is a key regulator of cell size,[78] we created clonal populations of *Tor*^{RNAi} cells in the posterior medial region of the tissue. As expected, these cells exhibited a reduction in apical area (Figures S6A and S6B), and we turned our attention to the first (R1) and second (R2) rows of WT cells around *Tor*^{RNAi} clones (Figure 7A). R1 cells are in direct contact with small *Tor*^{RNAi} cells, and we found their relative areas to be typically bigger than those of R2 cells (Figure 7B, left bar). If a

released over 30 min to carry out a ∼15% uniaxial compaction (arrow). In non-compacted pupae, the PDMS was not released. In compacted and non-compacted pupae, Ecad:3xGFP signal was then acquired every 5 min until 30 hAPF to record the dynamics of the tissue. See also STAR Methods for details. Analyses are made in the posterior medial region of the notum (red box, bottom sketch).

(B and C) Distributions of cell apical areas (B, mean ± SEM), and cell relative apical areas (C, mean ± SEM) of cells at 18h15 APF in compacted (dark blue, n = 4,317 cells from N = 3 nota) and non-compacted nota (gray, n = 4,905 cells from N = 3 nota). Curves are smoothed over 3 points. The area below each curve is set to one. Dashed lines: average values. Apical area, $p = 1.2 \times 10^{-105}$ and relative area, p = 0.94, Student's t tests.

(D) Graph of the fold change in apoptosis rate (mean ± SEM) induced by compaction between 18 and 32 hAPF, predicted (blue, prediction made in N = 3 non-compacted nota, n = 4,617 cells and compared with the corresponding experimental rate) versus experimental fold change (dark blue, N = 3 compacted nota, n = 4,055 cells; same data used for prediction for non-compacted animals). p = 0.82, Student's t test.

(E) Graph of the predicted fold change in apoptosis rate predicted to occur between 18 and 32 hAPF following a 19% tissue compaction, corresponding to the observed experimental cell apical area reduction, in N = 3 non-compacted animals. For each notum, three categories of apoptosis are shown: apoptosis predicted without compaction (gray), compaction-induced apoptosis predicted in the apoptosis mask (blue), or compaction-induced apoptosis outside the apoptosis mask (yellow). The values are normalized by the number of apoptoses predicted without compaction. From left to right: n = 1,618; 1,393; and 1,606 cells.

(F) Apoptosis maps in non-compacted (top) and compacted (bottom) tissues at 20 hAPF, with the apoptosis mask outlined by thick dashed red lines. Nota cells are color coded according to the upcoming number of apoptoses in their progeny (white: no extrusion, black: at least 3 extrusions). Magenta dashed line: midline. Magenta dots: macrochaetae.

(G) Boxplot of the cell area relative variations between t = 0 and t = 30 min versus the initial cell area for non-compacted (gray, n = 8,501 cells in N = 3 nota) and compacted nota (blue, n = 6,952 cells from N = 3 nota). The box represents the interquartile range (between the 1st and the 3rd quartile). Each whisker represents 1.5 times the interquartile range. The red line represents the median. Cells are binned in 10-μm^2-wide bins between 10 and 60 μm^2. p values between non-compacted and compacted in each area bin: 2.0×10^{-8} (10–20 μm^2), 2.6×10^{-31} (20–30 μm^2), 1.5×10^{-60} (30–40 μm^2), 2.0×10^{-48} (40–50 μm^2), 3.6×10^{-9} (50–60 μm^2), Kolmogorov-Smirnov test; p value between the 1st bin (10–20 μm^2) and the last bin (50–60 μm^2) for compacted cells: 1.2×10^{-40}, Kolmogorov-Smirnov test.

(H) Boxplot of the apoptosis rates versus cell initial areas (namely before compaction) in non-compacted (gray, n = 4,289 cells in N = 3 nota) and compacted nota (blue, n = 3,190 cells from N = 3 nota). The box represents the interquartile range (between the 1st and the 3rd quartile). Each whisker represents 1.5 times the interquartile range. The red line represents the median. p values between non-compacted and compacted in each area bin: 0.033 (0–20 μm^2), 0.033 (20–40 μm^2), 0.32 (40–60 μm^2), Kolmogorov-Smirnov test; p value between the 1st bin (0–20 μm^2) and the last bin (40–60 μm^2) for compacted cells: 0.033, Kolmogorov-Smirnov test.

Scale bars: 50 μm. NS $p \geq 0.05$; *$p < 0.05$; ****$p < 0.0001$.

See also Figure S4 and Table S2.

Please cite this article in press as: Cachoux et al., Epithelial apoptotic pattern emerges from global and local regulation by cell apical area, Current Biology (2023), https://doi.org/10.1016/j.cub.2023.09.049

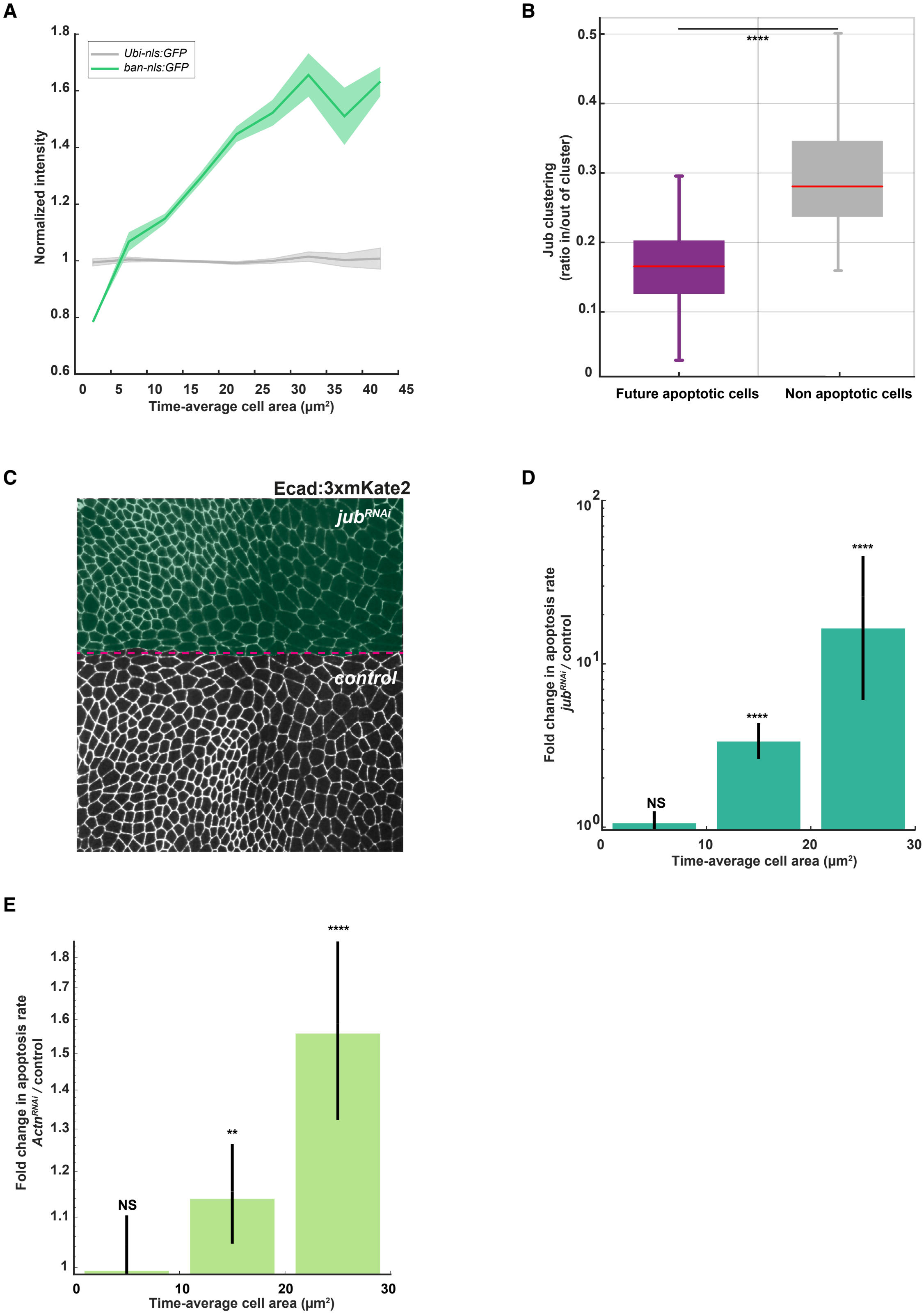

Figure 6. Linking Hippo/YAP signaling, apoptosis and apical cell area

(A) Graph of Ban-nls:GFP (green, n = 1,228 cells from N = 2 nota) and Ubi-nls:GFP (gray, n = 1,233 cells from N = 2 nota) signals (mean ± SEM) versus cell apical area. Cells are binned in 5-μm^2-wide bins from 0 to 45 μm^2. Data points are from López-Gay et al.[43]

(legend continued on next page)

bigger relative area impedes cell death, we expect apoptosis to be decreased in these WT cells, whereas if R1 and R2 cells have similar apoptosis rate, it would suggest that the increased relative area of R1 cells does not impact apoptosis. We found that, at constant cell size, R1 WT cells have a 20% lower probability to enter apoptosis, as compared with R2 WT cells (Figure 7C, left bar), consistent with a role for relative area in modulating apoptosis. We also verified the role of relative area within the Tor^{RNAi} clones: Tor^{RNAi} cells on the clone border, in contact with WT cells, are characterized by smaller relative areas than Tor^{RNAi} cells in the clone bulk (Figure 7B, right bar). As expected, we find that these border clone cells die significantly more than the bulk clone cells (Figure 7C, right bar). Overall, these results suggest that the modulation of cell relative apical area impacts apoptosis and thus prompted us to explore whether signaling pathways are involved in this regulation.

Notch signaling is required for the regulation of apoptosis by the cell relative apical area

To identify the molecular pathways involved in the preferential death of cells apically smaller than their neighbors, we initially hypothesized that such preferential death might relate to a context-dependent form of cell elimination, which involves comparison with adjacent cells. As such, it might share characteristics with contact-dependent cell competition mechanisms.[79–84] To explore this hypothesis, we analyzed the role of the *azot* gene that mediates numerous forms of cell competition in the *Drosophila* wing imaginal disc and pupal retina, as well as the adult fly brain and gut.[85] We abrogated *azot* function and studied the impact on apoptosis in the posterior region of the notum. In *azot* tissue, we found that the pattern of apoptosis is preserved (Figure S6C) and that apoptotic cells are 11% ± 2.6% apically smaller than their neighbors, comparable to the 12% ± 3.2% difference seen in control tissues (Figure S6D). Therefore, the loss of Azot function did not alter the relationship between cell apoptosis and cell relative area. This finding indicates that the elimination of cells smaller than their neighbors is not regulated by Azot. Since the mechanisms of cell competition are very diverse,[79–81,84] our study of *azot* does not exclude the possibility that death mediated by cell relative area is connected to a form of endogenous cell competition (see also discussion). Yet, it prompted us to investigate other pathways by which the relative apical areas of cells could impact their survival.

We decided to test the possible involvement of the Notch pathway in the regulation of apoptosis by cell relative area. Notch regulates lateral inhibition, a process driving differential fate decisions between neighboring cells in a large variety of living systems.[86–88] Notch signaling also impacts cell death, promoting either pro-apoptotic or anti-apoptotic activity in a context-dependent manner.[89,90] In addition, *Notch* signaling correlates with the cell-cell contact area in *in vitro* contact assays of pairs of epithelial cells.[91] Nevertheless, its role in the regulation of cell survival as a function of relative area has not been explored. To investigate the role of this pathway, we used a temperature-sensitive Notch allele ($Notch^{ts}$) to specifically block Notch function during pupal development. Focusing on the posterior medial region of the notum, we found that the relative apical area of apoptotic cells is higher in $Notch^{ts}$ condition than in control condition, and this is seen throughout their lives, as early as 8 h before apoptosis (Figure 7D). To verify that cell extrusion in $Notch^{ts}$ tissue is apoptotic, we used the GC3Ai caspase reporter and found that out of 110 extruding $Notch^{ts}$ cells, all exhibited a burst of caspase activity before their extrusion (Figure S7A; Video S5A). Importantly, the apoptotic pattern and distribution of relative areas are identical in control and $Notch^{ts}$ conditions (Figures S7B, S7C, and S7E). In agreement with the reported binding of Su(H) to the *Diap1* promoter,[92] we found that the level of the *Diap1-nls:GFP* reporter was reduced in $Notch^{RNAi}$ clones, thereby further confirming a role of Notch signaling in regulating apoptosis (Figure S7F, left). Furthermore, this regulation is likely independent of Hippo/YAP signaling, since *ban-nls:GFP* was not affected in $Notch^{RNAi}$ clones (Figure S7F, right) and since jub^{RNAi} did not impact the preferential death of cells smaller than their neighbors (Figure S5I). Moreover, and as opposed to jub^{RNAi} and $Actn^{RNAi}$, inhibiting Notch function did not significantly impact the relationship between cell apical area and the apoptosis probability (Figure S7G). Collectively, these results indicate that Notch signaling is necessary to ensure the modulation of apoptosis by cell relative apical size.

To regulate death according to relative area, Notch signaling could either sense the relative cell area or coordinate cell death between neighboring cells. To explore these two possibilities, we analyzed the level of a well-established transcriptional Notch reporter (*NRE-nls:mChFP*[93]) as a function of cell relative apical area. We found that the level of this Notch reporter does not correlate with relative area (Figures S7H and S7I). In contrast, when specifically analyzing future apoptotic cells prior to their death, we found that the Notch reporter level was slightly lower in the apoptotic cells than in its neighbor cells, whereas a control nls:RFP reporter expressed under an ubiquitin promoter accumulated at similar level in the apoptotic cells and its neighbors (Figures 7E and 7F). Together, this suggests that Notch signaling

---

(B) Boxplot of Jub:GFP clustering measured as the ratio between the junctional Jub:GFP signal inside clusters versus outside cluster in future apoptotic and in their surrounding non-apoptotic cells. The box represents the interquartile range (between the 1st and the 3rd quartile). Each whisker represents 1.5 times the interquartile range. The red line represents the median. n = 96 future apoptotic cells and 96 non-apoptotic cells (N = 2 nota). p value: 10^{-8}, Mann-Whitney U test.

(C) Image of Ecad:3xmKate2 in the posterior medial notum harboring a jub^{RNAi} clone (green, marked by Caax:BPF, not shown) as well as the contralateral symmetric control cells. Magenta dashed line: midline.

(D) Graph of the fold change in apoptosis rate between jub^{RNAi} clones and contralateral control cells versus cell apical area. n = 1,469 for control cells and n = 1,254 for jub^{RNAi} cells from N = 4 nota. Log-scale. Error bar: 95%, confidence interval (CI), Fisher test. p values: 0.37 (0–10 μm^2), 5.6×10^{-33} (10–20 μm^2), 8.2×10^{-16} (20–30 μm^2), Fisher test.

(E) Graph of the fold change in apoptosis rate between $Actn^{RNAi}$ and control (w^{RNAi}) cells versus cell apical area. n = 1,767 cells from $pnr\text{-}Gal4>Actn^{dsRNA}$ nota (N = 5) and somatic $Actn^{RNAi}$ clones (N = 2 nota); n = 2,729 control cells from $pnr\text{-}Gal4>w^{dsRNA}$ nota (N = 5), somatic w^{RNAi} clones (N = 2 nota). Error bar: 95% CI, Fisher test. p values: 1 (0–10 μm^2), 1.4×10^{-3} (10–20 μm^2), 1.6×10^{-8} (20–30 μm^2), Fisher test.

Scale bars: 10 μm. NS $p \geq 0.05$; $^{**}p < 0.01$; $^{****}p < 0.0001$. Clone induction regimes are described in STAR Methods.

See also Figures S5 and S6, and Table S2.

Please cite this article in press as: Cachoux et al., Epithelial apoptotic pattern emerges from global and local regulation by cell apical area, Current Biology (2023), https://doi.org/10.1016/j.cub.2023.09.049

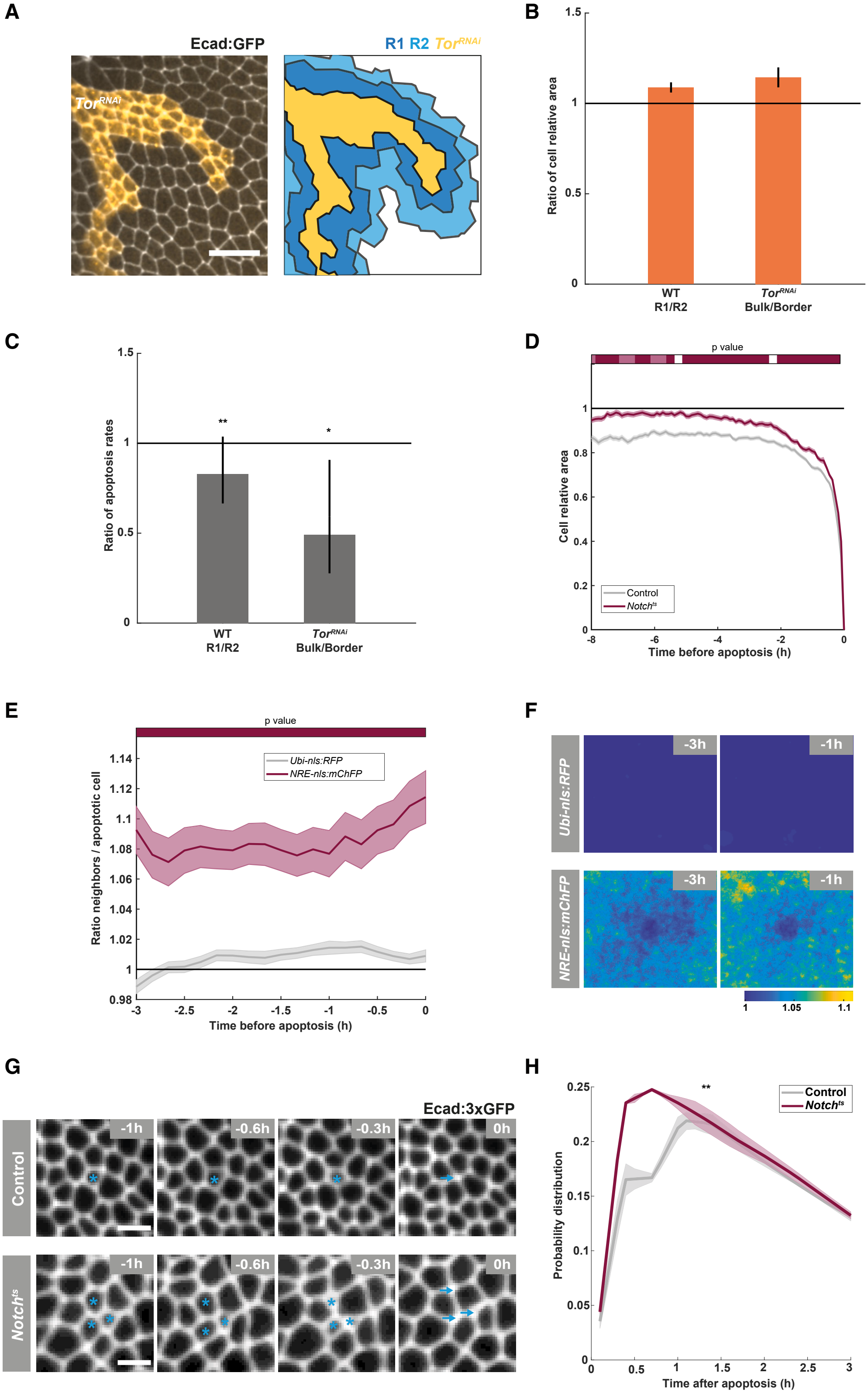

Figure 7. Roles of cell relative area and Notch signaling in apoptosis

(A) Left: close-up of an Ecad:3xGFP notum with a Tor^{RNAi} clone (yellow) at 15 hAPF. Right: schematic representation of the same region, with the clone cell outlines in yellow, first row neighbors (R1) in dark blue, and second row neighbors (R2) in light blue. Tor^{RNAi} clones are marked by Caax:BFP (yellow).

(legend continued on next page)

Please cite this article in press as: Cachoux et al., Epithelial apoptotic pattern emerges from global and local regulation by cell apical area, Current Biology (2023), https://doi.org/10.1016/j.cub.2023.09.049

is differentially activated in cells fated to die due to their relative size to coordinate the death among neighbor cells. Accordingly, in $Notch^{ts}$ tissue, we noticed the presence of apoptosis clusters usually not seen in epithelial tissues (Figure 7G; Video S5B). Notably, this is associated neither with a reduction in cell area, since the cell areas are larger by 8% in $Notch^{ts}$ conditions ($37.3\ \mu m^2$ in control versus $40\ \mu m^2$ in $Notch^{ts}$ tissues), nor with a change in relative areas (Figures S7C–S7E). To quantify the occurrence of clusters, for every apoptosis, we measured subsequent apoptoses occurring in a 5-μm radius (corresponding approximately to direct neighbors) and 3-h time window around the initial apoptotic cell. In agreement with a role of Notch in coordinating cell death depending on cell relative area, we found that inhibiting Notch leads to a significant increase in the probability of observing a nearby apoptosis in a 0.5–1.5 h time window after an apoptosis (Figure 7H). Together, these results uncovered a role of Notch signaling in the regulation of apoptosis by cell relative apical area, which involves contributing to the local coordination of apoptosis between neighboring cells, thereby preventing the occurrence of apoptotic cell clusters.

DISCUSSION

During development and homeostasis, apoptosis plays a crucial role in defining tissue cell number and architecture, and the deregulation of apoptosis can lead to severe organ shape defects or diseases.[9,10,21,49,80] The genetic and biochemical regulations contributing to apoptosis have been extensively described.[9,10,94] In addition, numerous studies have delineated how caspase activation, cell-cell adhesion, and cytoskeleton remodeling promote the cell shape changes associated with cell extrusion in epithelial tissues.[11–19] Here, we explored the role of cell geometry in controlling the spatial pattern of epithelial apoptosis during development. By analyzing the apoptotic pattern at the tissue scale, we uncovered two distinct processes of geometric control of cell death, both involving cell apical area but acting at different scales: (1) globally, at the tissue level, regions displaying cells with smaller areas define likely apoptotic zones and (2) locally, at the cell level, the relative area modulates the rate of apoptosis, thereby determining probable apoptotic cells. Thus, our work uncovered a relationship between programmed cell death and geometry shaping the tissue-scale apoptotic pattern.

Previous investigations on the regulation of apoptosis by biophysical factors have used genetic or mechanical ectopic tissue compressions to investigate the impact of biophysical factors on cell death. In particular, tissue contraction, which is linked to dynamic changes of cell size, was suggested to drive the apoptosis of WT cells.[31–33,35] We have observed that the physiological contractions of the tissue cannot fully explain the apoptotic pattern. In accordance with this finding, exerting a homogeneous compaction on developing pupae resulted in a non-homogeneous increase in apoptosis. The important factor is apical cell size, whose dynamics and relative value compared with the cell neighbors are distinct in future apoptotic and non-apoptotic cells early in their lives, hours before apoptosis. In collective assemblies of cells in culture, topological defects can locally specify cell death.[34] Here, we found that cells fated to die are characterized by a smaller area than the other cells in the tissue and by a relative area smaller than their direct neighbors. Thus, our work uncovered an additional non-autonomous geometrical regulation of cell apoptosis in tissue. Overall, by scrutinizing the correlation among endogenous tissue movements, cell geometry, and apoptosis, our findings deepen our understanding of the link between tissue contraction and apoptosis in developing tissue and explicitly enunciate how cell area and relative area can

(B) Graph of the ratios of the mean relative areas for (i) R1 and R2 control cells neighboring Tor^{RNAi} clones (1.09 ± 0.01, left) and (ii) bulk and border Tor^{RNAi} clone cells (1.14 ± 0.03, right). WT cells: n = 1,568 R1 and 1,903 R2 cells.[2] Tor^{RNAi} clone cells: 181 bulk cells and 871 border cells. n = 10 clones from N = 2 nota. Error bar: 95% CI.

(C) Graph of the ratio of apoptosis rates occurring in (i) R1 and R2 control cells neighboring Tor^{RNAi} clones (left), where a significant impact of relative area on cell death was found (p = 0.003, likelihood ratio statistic test), and (ii) bulk and border Tor^{RNAi} clone cells (right), where a significant impact of relative area on cell death was found as well (p = 0.011, likelihood ratio statistic test). See STAR Methods for statistical analysis. WT cells: 1,568 R1 and 1,903 R2 cells. Tor^{RNAi} clone cells: 181 bulk cells and 871 border cells n = 10 clones from N = 2 nota. Error bar: 95% CI, Fisher test.

(D) Graph of the relative apical area of apoptotic cells (mean ± SEM) versus time before apical extrusion in $Notch^{ts}$ (dark red, n = 1,327 cells from N = 3 nota) and control tissues between 16 and 35 hAPF (gray, n = 1,417 cells from N = 2 nota). Time evolutions of single cell relative areas have been aligned to their time of apical extrusion set to t = 0 and averaged. Horizontal bar: p values of Student's t tests performed between $Notch^{ts}$ and the control tissues every 15 min (color code: white, $p \geq 0.05$; light red, $p < 0.05$, dark red $p < 0.01$). Logistic regression shows that a decrease in relative area by 0.1 corresponds to an 8.2% increase in the apoptosis rate in control cells versus a 4.2% increase in $Notch^{ts}$ cells: the coefficient of correlation between relative apical area and apoptosis, which measures the strength of the relationship between these two factors, is decreased 2-fold when Notch is inhibited (-1.74 in control versus -0.55 in $Notch^{ts}$ tissues).

(E) Graph of the ratios of the *NRE-nls:mChFP* reporter activity (dark red, n = 24 apoptosis and their 100 neighbors, N = 2 nota) and Ubi-nls:RFP (gray, n = 24 apoptotic cells and their 72 neighbors from N = 2 nota) in cells neighboring apoptotic cells over the activity of the corresponding apoptotic cells during the 3 h before apoptosis. Horizontal bar: p values of Student's t tests performed between *NRE-nls:mChFP* and Ubi-nls:RFP cells every 15 min (color code: dark red $p < 0.01$).

(F) Averaged normalized Ubi-nls:RFP (top) and *NRE-nls:mChFP* (bottom) signals in a $24 \times 24\ \mu m^2$ region around the future apoptotic cells. Results shown at 3 h (n = 531 apoptotic cells, N = 2 nota, and n = 205 apoptotic cells, N = 2 nota, for *NRE-nls:mChFP* and *Ubi-nls:RFP*, respectively) and 1 h (n = 553 apoptotic cells, N = 2 nota, and n = 282 apoptotic cells, N = 2 nota for *NRE-nls:mChFP* and *Ubi-nls:RFP*, respectively) before apoptosis. The activity is normalized by the average value in the central 100 pixels.

(G) Ecad:3xGFP time-lapse images of apoptotic cells in control (top) and $Notch^{ts}$ (bottom) nota illustrating the presence of clusters of apoptotic cells in $Notch^{ts}$ nota. Cyan asterisks: apoptotic cells. Cyan arrows: position of the extruded cells. Time (h) is set to 0 at the time of apical extrusion.

(H) Graph of the temporal distribution of neighboring apoptosis following the apoptosis of a cell in $Notch^{ts}$ (dark red, mean ± SEM, n = 2,469 cells from N = 3 nota) and control (gray, mean ± SEM, n = 1,328 cells from N = 2 nota). Time is set to 0 at the time of the apoptosis of the cell of interest. Neighboring apoptosis are detected in a $5\ \mu m^2$ radius. A significant increase in the probability of a nearby apoptosis in the 0.5–1.5 h time window is observed: p = 0.002, Fisher test.

Scale bars: 20 μm (A), 5 μm (G). * p <0.05; ** p< 0.01. Clone induction regimes are described in STAR Methods.

See also Figures S6 and S7, Video S5, and Table S2.

Please cite this article in press as: Cachoux et al., Epithelial apoptotic pattern emerges from global and local regulation by cell apical area, Current Biology (2023), https://doi.org/10.1016/j.cub.2023.09.049

instruct the patterns of tissue apoptosis. Previous studies have shown that epithelial cell apical geometry is controlled by the balance between cortical tension and cell-cell adhesion.[95] We envision that the initial pattern of cell geometry within the notum is dependent on the activity patterns of cortical tension regulators and the expression of cell-cell adhesion molecules. Overall, the biophysical mechanisms regulating apoptosis can be influenced by tissue compression,[31–33,35] cell topology,[34] or cell area (this study). It will be interesting to investigate in contexts where tissue compression has been shown to control cell death whether area or relative area can also influence cell apoptosis. We foresee that in the future, it will be crucial to explore the respective roles of tissue mechanical force and cell geometry and to determine whether and how local cell-cell interactions could contribute to tissue-scale apoptotic patterns in other contexts.

Past and recent studies have investigated how cell geometry correlates to or modulates cell fate acquisition or differentiation,[52–55,91,96–99] therefore calling for the characterization of the link between cell morphology and signaling pathways regulation. Here, by exploring the role of cell geometry in apoptosis in the posterior medial region of the tissue, we have found that the Hippo/YAP and Notch signaling pathways mediate the links between two geometric properties of epithelial cells and apoptosis. By building on our previous work showing that apical stress fibers form in response to mechanical stress[43] and by analyzing the role of Ajuba and α-Actinin, we found that in the posterior central region of the notum, the cell-autonomous control of apoptosis by cell apical area involves the Hippo/YAP pathway. We propose that such control is linked to the formation of apical stress fibers in response to mechanical stress, since α-actinin is needed for stress fiber formation.[43] Although modulating cell area by adjusting the proliferation rate suggests that cell apical area can be a determinant of cell death throughout the notum, we have confined our functional analysis to the posterior central region where we have previously established a link between Hippo/YAP signaling and cell area under mechanical stress. Future mechanistic studies will be needed to comprehend how small apical area can induce apoptosis in other regions of the tissue. Notably, since the highly conserved Hippo/YAP pathway is a critical actor of apoptosis in multiple contexts and a known effector of mechanical forces or actomyosin organization that impact cell shape,[9,100,101] a similar control of apoptosis by cell geometry could take place in other tissues. Then, we showed that the local modulation of apoptosis by relative apical area requires Notch function. Depending on cell types, the Notch pathway has been found to have pro- or anti-apoptotic activity[9]; moreover, previous works have established that Notch signaling increases with cell contact length *in vitro*, a scaling that was proposed to entail a regulation of Notch by cell area.[91] Here, using a reporter of Notch transcriptional activity, we observed that future apoptotic cells, which are smaller than their neighbors, are characterized by reduced Notch transcriptional activity but that Notch reporter level does not correlate with the cell relative area at tissue scale. Therefore, prior to the choice of the apoptotic cell, the differences in Notch transcriptional output might be too low to be detected using this reporter, or Notch signaling is rather acting to prevent the death of larger neighbor cells once the apoptotic cell has been selected. Interestingly, recent studies highlighted the various and context-dependent modes of interplay between Notch and Hippo/YAP signaling in the control of cell fate decisions.[102,103] We found that Hippo/YAP and Notch signaling pathways have an additional interplay, as they both modulate cell apoptosis in response to two distinct geometric characteristics. Last, we envision that Notch and ERK signaling might cooperate in the local control of apoptosis. We found that Notch activity prevents the occurrence of clusters of apoptotic cells dying together by diminishing the probability to die in the neighbors of an apoptotic cell between 0.5 and 1.5 h after apoptosis. This timing is consistent with the time window recently found to correspond to the local and transient restriction of apoptosis in the neighbors of an apoptotic cell by ERK activation.[104,105] As Notch signaling is differentially activated in the future apoptotic cell prior to apoptosis, whereas ERK signaling is triggered in the neighbors of cells upon apoptosis, the Notch and ERK pathways could, respectively, act prior and after cell delamination to locally tune apoptosis and avoid the disruption of tissue integrity. Notch and EGFR (Epidermal Growth Factor Receptor) have been shown to control cell apoptosis in multiple developmental contexts.[9] It will be relevant to test whether their interplay stems from a geometric control of cell apoptosis. Overall, by delineating the link between the geometrical control of apoptosis and signaling pathways in developing tissues, our work enhances the understanding of the mechanisms by which cell geometry modulates cell fate and dynamics.

Cell apoptosis has been associated with the fundamental process of cell competition.[79–84] We have established that within regions of small cells, cells that are even smaller than the surrounding cells are more likely to be eliminated, thus freeing some space for larger cells. One can consequently wonder whether our work uncovers a form of endogenous cell competition linked to cell apical area and relative area. Cell competition broadly refers to the biological process whereby the death of ‘‘loser’’ cells by ‘‘winner’’ cells is context dependent, i.e., loser cells are fully viable if not challenged by the presence of winner cells. The underlying mechanisms promoting the loser/winner status are rooted to insufficient extracellular pro-survival factors, communication via cell-cell contact, or mechanical stress.[79–84] In particular, mechanical cell competition entails the variation of cell sensitivity in response to cell crowding due to genetic mosaicism[32,80,81,106]; loser cells are more sensitive to mechanical compaction and are more likely to die due to compressive forces imposed by surrounding winner cells.[32,37,106] Genetic mosaicisms for the tumor suppressor Scrib in cell lines, the oncogenic Ras expression in *Drosophila*, or megabase genomic rearrangements in human pluripotent stem cells lead to differences in sensitivity to mechanical compaction and death.[32,37,106] Here, we observed that endogenous cell death is predicted by smaller area and relative cell area, two processes mediated by the Hippo/YAP and Notch pathways, respectively. Since the ectopic genetic modulations of Notch and Hippo/YAP signaling have been associated with cell competition,[107–110] we envision that our work could concur with our understanding of cell competition. First, it strengthens the notion that cell crowding can be a factor contributing to the sensitivity of cells to mechanical competition induced by genetic mosaicism. Second, by delineating that cells smaller than their neighbors are more likely to be eliminated, our findings can be framed as a form of

Please cite this article in press as: Cachoux et al., Epithelial apoptotic pattern emerges from global and local regulation by cell apical area, Current Biology (2023), https://doi.org/10.1016/j.cub.2023.09.049

endogenous "geometric cell competition," whereby (1) the smaller area and relative area via Hippo/YAP and Notch pathways link to a loser/winner cell status and (2) the death of smaller cells leaves more space to bigger ones, which thus become even larger. Overall, by establishing a critical role for cell geometry in the control of apoptosis during development, our findings suggest parallel roles of cell geometry in the control of cell competition and developmental apoptosis.

Tissue development and homeostasis rely on the balance between proliferation and apoptosis. Numerous works have investigated the critical role of cell geometry in cell-cycle progression and cell division orientation to understand the regulation of tissue size, organization, and shape.[4–7] Our work now establishes that two geometric cell features related to apical size are associated with apoptosis and are sufficient to recapitulate the apoptotic pattern in a developing tissue with good accuracy. Interestingly, apoptosis and proliferation, in turn, modulate cytoskeleton organization, tissue mechanics, and signaling, which are potent regulators of cell and tissue geometrical features. Therefore, we foresee that integrating the role of geometry in the control of apoptosis and cell division will be instrumental to fully understand how tissue cell number, size, shape, and architecture are regulated or maintained.

STAR★METHODS

Detailed methods are provided in the online version of this paper and include the following:

- KEY RESOURCES TABLE
- RESOURCE AVAILABILITY
  - Lead contact
  - Materials availability
  - Data and code availability
- EXPERIMENTAL MODEL AND SUBJECT DETAILS
  - Fly husbandry and stocks
- METHOD DETAILS
  - Genetics
  - Generation of ERK KTR:GFP transgenic reporter
  - Pupa and adult mounting and imaging
  - Prediction model
- QUANTIFICATION AND STATISTICAL ANALYSIS
  - Quantifications of tissue dynamics
  - Quantification of fluorescent reporter
  - Statistics

SUPPLEMENTAL INFORMATION

Supplemental information can be found online at https://doi.org/10.1016/j.cub.2023.09.049.

ACKNOWLEDGMENTS

We thank M. Gho, Y. Hong, M. Milan, E. Moreno, M. Suzanne, the Bloomington, Vienna, Harvard Medical School Stock Centers, and the Developmental Studies Hybridoma Bank for reagents; the PICT-IBiSA@BDD imaging facility (ANR-10-INBS-04); L. Alpar, A. Bardin, F. Graner, B. Lefèvre, J-L. Maitre, and R. Sheshka for comments; C. Kana Tepakbong, L. Sancéré, and C. Barbier for help with segmentation; O. Renaud and O. Leroy for help with ablation; and A. Dauphin for laser power measurements. This work was supported by Institut Curie, CNRS, INSERM, ERC Advanced Scaling-Sensitivity (101020243), ARC (SL220130607097), ANR (TiMecaDiv 20CE13000801), ANR (ChronoDamage 20CE13-0013), CANCERO-INCA (PLBIO2020/BELLAICHE), and ANR Labex DEEP (11-LBX-0044, ANR-10-IDEX-0001-02). V.M.L.C., M.G., F.d.P. and A.M. acknowledge FRM (FDT201805005805, FDT202106013046, and SPF202005011933) and ARC (PDF20181208399) fellowships, respectively.

AUTHOR CONTRIBUTIONS

V.M.L.C., M.B., B.G., and Y.B. designed the project. I.G. and M.B. produced reagents. M.B., M.G., F.B., J.M.L.-G., A.M., and F.d.P. developed experimental methods or performed experiments. V.M.L.C., S.R., and B.G. developed data analysis methods and quantification scripts. V.M.L.C., M.B., M.G., L.N., and B.G. analyzed the data. V.M.L.C., M.G., B.G., and Y.B. wrote the manuscript and designed the figures.

DECLARATION OF INTERESTS

The authors declare no competing interests.

Received: April 21, 2023
Revised: August 7, 2023
Accepted: September 20, 2023
Published: October 11, 2023

REFERENCES

1. Ansari, B., and Hall, P.A. (1992). The kinetic organisation of tissues. In Assessment of Cell Proliferation in Clinical Practice (Springer). https://doi.org/10.1007/978-1-4471-3190-8_3.
2. Villars, A., and Levayer, R. (2022). Collective effects in epithelial cell death and cell extrusion. Curr. Opin. Genet. Dev. *72*, 8–14. https://doi.org/10.1016/j.gde.2021.09.004.
3. Foster, J.R. (2000). Cell death and cell proliferation in the control of normal and neoplastic tissue growth. Toxicol. Pathol. *28*, 441–446.
4. Amodeo, A.A., and Skotheim, J.M. (2016). Cell-size control. Cold Spring Harb. Perspect. Biol. *8*, a019083.
5. Levy, D.L., and Heald, R. (2016). Biological scaling problems and solutions in amphibians. Cold Spring Harb. Perspect. Biol. *8*, 1–16. https://doi.org/10.1101/cshperspect.a019166.
6. Haupt, A., and Minc, N. (2018). How cells sense their own shape - mechanisms to probe cell geometry and their implications in cellular organization and function. J. Cell Sci. *131*, https://doi.org/10.1242/jcs.214015.
7. Lechler, T., and Mapelli, M. (2021). Spindle positioning and its impact on vertebrate tissue architecture and cell fate. Nat. Rev. Mol. Cell Biol. *22*, 691–708. https://doi.org/10.1038/S41580-021-00384-4.
8. Li, J., and Yuan, J. (2008). Caspases in apoptosis and beyond. Oncogene *27*, 6194–6206. https://doi.org/10.1038/onc.2008.297.
9. Arya, R., and White, K. (2015). Cell death in development: signaling pathways and core mechanisms. Semin. Cell Dev. Biol. *39*, 12–19. https://doi.org/10.1016/j.semcdb.2015.02.001.
10. Fuchs, Y., and Steller, H. (2011). Programmed cell death in animal development and disease. Cell *147*, 742–758. https://doi.org/10.1016/J.CELL.2011.10.033.
11. Ambrosini, A., Rayer, M., Monier, B., and Suzanne, M. (2019). Mechanical function of the nucleus in force generation during epithelial morphogenesis. Dev. Cell *50*, 197–211.e5. https://doi.org/10.1016/J.DEVCEL.2019.05.027.
12. Duszyc, K., Gomez, G.A., Lagendijk, A.K., Yau, M.K., Nanavati, B.N., Gliddon, B.L., Hall, T.E., Verma, S., Hogan, B.M., Pitson, S.M., et al. (2021). Mechanotransduction activates RhoA in the neighbors of apoptotic epithelial cells to engage apical extrusion. Curr. Biol. *31*, 1326–1336.e5. https://doi.org/10.1016/j.cub.2021.01.003.
13. Michael, M., Meiring, J.C.M., Acharya, B.R., Matthews, D.R., Verma, S., Han, S.P., Hill, M.M., Parton, R.G., Gomez, G.A., and Yap, A.S. (2016).

Coronin 1B reorganizes the architecture of F-actin networks for contractility at steady-state and apoptotic adherens junctions. Dev. Cell *37*, 58–71. https://doi.org/10.1016/j.devcel.2016.03.008.

14. Teng, X., Qin, L., le Borgne, R., and Toyama, Y. (2017). Remodeling of adhesion and modulation of mechanical tensile forces during apoptosis in Drosophila epithelium. Development *144*, 95–105. https://doi.org/10.1242/DEV.139865.
15. Grieve, A.G., and Rabouille, C. (2014). Extracellular cleavage of E-cadherin promotes epithelial cell extrusion. J. Cell Sci. *127*, 3331–3346. https://doi.org/10.1242/JCS.147926.
16. Le, A.P., Rupprecht, J.F., Mège, R.M., Toyama, Y., Lim, C.T., and Ladoux, B. (2021). Adhesion-mediated heterogeneous actin organization governs apoptotic cell extrusion. Nat. Commun. *12*, 397. https://doi.org/10.1038/S41467-020-20563-9.
17. Atieh, Y., Wyatt, T., Zaske, A.M., and Eisenhoffer, G.T. (2021). Pulsatile contractions promote apoptotic cell extrusion in epithelial tissues. Curr. Biol. *31*, 1129–1140.e4. https://doi.org/10.1016/J.CUB.2020.12.005.
18. Kuipers, D., Mehonic, A., Kajita, M., Peter, L., Fujita, Y., Duke, T., Charras, G., and Gale, J.E. (2014). Epithelial repair is a two-stage process driven first by dying cells and then by their neighbours. J. Cell Sci. *127*, 1229–1241. https://doi.org/10.1242/JCS.138289.
19. Villars, A., Matamoro-Vidal, A., Levillayer, F., and Levayer, R. (2022). Microtubule disassembly by caspases is an important rate-limiting step of cell extrusion. Nat. Commun. *13*, 3632. https://doi.org/10.1038/s41467-022-31266-8.
20. Rosenblatt, J., Raff, M.C., and Cramer, L.P. (2001). An epithelial cell destined for apoptosis signals its neighbors to extrude it by an actin- and myosin-dependent mechanism. Curr. Biol. *11*, 1847–1857.
21. Ohsawa, S., Vaughen, J., and Igaki, T. (2018). Cell extrusion: a stress-responsive force for good or evil in epithelial homeostasis. Dev. Cell *44*, 284–296. https://doi.org/10.1016/J.DEVCEL.2018.01.009.
22. Toyama, Y., Peralta, X.G., Wells, A.R., Kiehart, D.P., and Edwards, G.S. (2008). Apoptotic force and tissue dynamics during Drosophila embryogenesis. Science *321*, 1683–1686.
23. Cuervo, R., Valencia, C., Chandraratna, R.A.S., and Covarrubias, L. (2002). Programmed cell death is required for palate shelf fusion and is regulated by retinoic acid. Dev. Biol. *245*, 145–156. https://doi.org/10.1006/dbio.2002.0620.
24. Hernández-Martínez, R., and Covarrubias, L. (2011). Interdigital cell death function and regulation: new insights on an old programmed cell death model. Dev. Growth Differ. *53*, 245–258.
25. Monier, B., Gettings, M., Gay, G., Mangeat, T., Schott, S., Guarner, A., and Suzanne, M. (2015). Apico-basal forces exerted by apoptotic cells drive epithelium folding. Nature *518*, 245–248. https://doi.org/10.1038/nature14152.
26. Suzanne, M., Petzoldt, A.G., Spéder, P., Coutelis, J.B., Steller, H., and Noselli, S. (2010). Coupling of apoptosis and L/R patterning controls stepwise organ looping. Curr. Biol. *20*, 1773–1778. https://doi.org/10.1016/j.cub.2010.08.056.
27. Roellig, D., Theis, S., Proag, A., Allio, G., Bénazéraf, B., Gros, J., and Suzanne, M. (2022). Force-generating apoptotic cells orchestrate avian neural tube bending. Dev. Cell *57*, 707–718.e6. https://doi.org/10.1016/J.DEVCEL.2022.02.020.
28. Kawaue, T., Yow, I., Pan, Y., Le, A.P., Lou, Y., Loberas, M., Shagirov, M., Teng, X., Prost, J., Hiraiwa, T., et al. (2023). Inhomogeneous mechanotransduction defines the spatial pattern of apoptosis-induced compensatory proliferation. Dev. Cell *58*, 267–277.e5. https://doi.org/10.1016/J.DEVCEL.2023.01.005.
29. Ray, H.J., and Niswander, L. (2012). Mechanisms of tissue fusion during development. Development *139*, 1701–1711. https://doi.org/10.1242/DEV.068338.
30. Ranft, J., Basan, M., Elgeti, J., Joanny, J.F., Prost, J., and Jülicher, F. (2010). Fluidization of tissues by cell division and apoptosis. Proc. Natl. Acad. Sci. USA *107*, 20863–20868. https://doi.org/10.1073/pnas.1011086107.
31. Marinari, E., Mehonic, A., Curran, S., Gale, J., Duke, T., and Baum, B. (2012). Live-cell delamination counterbalances epithelial growth to limit tissue overcrowding. Nature *484*, 542–545. https://doi.org/10.1038/nature10984.
32. Levayer, R., Dupont, C., and Moreno, E. (2016). Tissue crowding induces caspase-dependent competition for space. Curr. Biol. *26*, 670–677. https://doi.org/10.1016/j.cub.2015.12.072.
33. Moreno, E., Valon, L., Levillayer, F., and Levayer, R. (2019). Competition for space induces cell elimination through compaction-driven ERK downregulation. Curr. Biol. *29*, 23–34.e8. https://doi.org/10.1016/j.cub.2018.11.007.
34. Saw, T.B., Doostmohammadi, A., Nier, V., Kocgozlu, L., Thampi, S., Toyama, Y., Marcq, P., Lim, C.T., Yeomans, J.M., and Ladoux, B. (2017). Topological defects in epithelia govern cell death and extrusion. Nature *544*, 212–216. https://doi.org/10.1038/nature21718.
35. Eisenhoffer, G.T., Loftus, P.D., Yoshigi, M., Otsuna, H., Chien, C.B., Morcos, P.A., and Rosenblatt, J. (2012). Crowding induces live cell extrusion to maintain homeostatic cell numbers in epithelia. Nature *484*, 546–549. https://doi.org/10.1038/nature10999.
36. Wagstaff, L., Goschorska, M., Kozyrska, K., Duclos, G., Kucinski, I., Chessel, A., Hampton-O'Neil, L., Bradshaw, C.R., Allen, G.E., Rawlins, E.L., et al. (2016). Mechanical cell competition kills cells via induction of lethal p53 levels. Nat. Commun. *7*, 11373. https://doi.org/10.1038/ncomms11373.
37. Price, C.J., Stavish, D., Gokhale, P.J., Stevenson, B.A., Sargeant, S., Lacey, J., Rodriguez, T.A., and Barbaric, I. (2021). Genetically variant human pluripotent stem cells selectively eliminate wild-type counterparts through YAP-mediated cell competition. Dev. Cell *56*, 2455–2470.e10. https://doi.org/10.1016/j.devcel.2021.07.019.
38. Martín-Blanco, E., Pastor-Pareja, J.C., and García-Bellido, A. (2000). JNK and decapentaplegic signaling control adhesiveness and cytoskeleton dynamics during thorax closure in Drosophila. Proc. Natl. Acad. Sci. USA *97*, 7888–7893. https://doi.org/10.1073/pnas.97.14.7888.
39. Guirao, B., Rigaud, S.U., Bosveld, F., Bailles, A., López-Gay, J., Ishihara, S., Sugimura, K., Graner, F., and Bellaïche, Y. (2015). Unified quantitative characterization of epithelial tissue development. eLife *4*, e08519. https://doi.org/10.7554/eLife.08519.
40. Bosveld, F., Bonnet, I., Guirao, B., Tlili, S., Wang, Z., Petitalot, A., Marchand, R., Bardet, P.L., Marcq, P., Graner, F., et al. (2012). Mechanical control of morphogenesis by Fat/Dachsous/Four-jointed planar cell polarity pathway. Science *336*, 724–727. https://doi.org/10.1126/science.1221071.
41. Founounou, N., Loyer, N., and le Borgne, R. (2013). Septins regulate the contractility of the actomyosin ring to enable adherens junction remodeling during cytokinesis of epithelial cells. Dev. Cell *24*, 242–255. https://doi.org/10.1016/j.devcel.2013.01.008.
42. Bosveld, F., Guirao, B., Wang, Z., Rivière, M., Bonnet, I., Graner, F., and Bellaïche, Y. (2016). Modulation of junction tension by tumor suppressors and proto-oncogenes regulates cell-cell contacts. Development *143*, 623–634. https://doi.org/10.1242/dev.127993.
43. López-Gay, J.M., Nunley, H., Spencer, M., di Pietro, F., Guirao, B., Bosveld, F., Markova, O., Gaugue, I., Pelletier, S., Lubensky, D.K., et al. (2020). Apical stress fibers enable a scaling between cell mechanical response and area in epithelial tissue. Science *370*, https://doi.org/10.1126/science.abb2169.
44. Antunes, M., Pereira, T., Cordeiro, J.V., Almeida, L., and Jacinto, A. (2013). Coordinated waves of actomyosin flow and apical cell constriction immediately after wounding. J. Cell Biol. *202*, 365–379. https://doi.org/10.1083/JCB.201211039.
45. Franz, A., Wood, W., and Martin, P. (2018). Fat body cells are motile and actively migrate to wounds to drive repair and prevent infection. Dev. Cell *44*, 460–470.e3. https://doi.org/10.1016/J.DEVCEL.2018.01.026.

46. Yoo, S.K., Pascoe, H.G., Pereira, T., Kondo, S., Jacinto, A., Zhang, X., and Hariharan, I.K. (2016). Plexins function in epithelial repair in both Drosophila and zebrafish. Nat. Commun. *7*, 12282. https://doi.org/10.1038/NCOMMS12282.

47. Fujisawa, Y., Shinoda, N., Chihara, T., and Miura, M. (2020). ROS regulate caspase-dependent cell delamination without apoptosis in the Drosophila pupal notum. iScience *23*, 101413. https://doi.org/10.1016/J.ISCI.2020.101413.

48. Fujisawa, Y., Kosakamoto, H., Chihara, T., and Miura, M. (2019). Non-apoptotic function of Drosophila caspase activation in epithelial thorax closure and wound healing. Development *146*, https://doi.org/10.1242/dev.169037.

49. Fadul, J., and Rosenblatt, J. (2018). The forces and fates of extruding cells. Curr. Opin. Cell Biol. *54*, 66–71. https://doi.org/10.1016/J.CEB.2018.04.007.

50. Schott, S., Ambrosini, A., Barbaste, A., Benassayag, C., Gracia, M., Proag, A., Rayer, M., Monier, B., and Suzanne, M. (2017). A fluorescent toolkit for spatiotemporal tracking of apoptotic cells in living Drosophila tissues. Development *144*, 3840–3846. https://doi.org/10.1242/dev.149807.

51. Siegrist, S.E., Haque, N.S., Chen, C.H., Hay, B.A., and Hariharan, I.K. (2010). Inactivation of both foxo and reaper promotes long-term adult neurogenesis in Drosophila. Curr. Biol. *20*, 643–648. https://doi.org/10.1016/j.cub.2010.01.060.

52. Chen, C.S., Mrksich, M., Huang, S., Whitesides, G.M., and Ingber, D.E. (1997). Geometric control of cell life and death. Science *276*, 1425–1428. https://doi.org/10.1126/science.276.5317.1425.

53. Mammoto, T., and Ingber, D.E. (2010). Mechanical control of tissue and organ development. Development *137*, 1407–1420. https://doi.org/10.1242/dev.024166.

54. Watt, F.M., Jordan, P.W., and O'Neill, C.H. (1988). Cell shape controls terminal differentiation of human epidermal keratinocytes. Proc. Natl. Acad. Sci. USA *85*, 5576–5580. https://doi.org/10.1073/PNAS.85.15.5576.

55. Folkman, J., and Moscona, A. (1978). Role of cell shape in growth control. Nature *273*, 345–349. https://doi.org/10.1038/273345a0.

56. Milán, M., Campuzano, S., and García-Bellido, A. (1996). Cell cycling and patterned cell proliferation in the Drosophila wing during metamorphosis. Proc. Natl. Acad. Sci. USA *93*, 11687–11692. https://doi.org/10.1073/pnas.93.21.11687.

57. Schubiger, M., and Palka, J. (1987). Changing spatial patterns of DNA replication in the developing wing of Drosophila. Dev. Biol. *123*, 145–153. https://doi.org/10.1016/0012-1606(87)90436-2.

58. Bosveld, F., Markova, O., Guirao, B., Martin, C., Wang, Z., Pierre, A., Balakireva, M., Gaugue, I., Ainslie, A., Christophorou, N., et al. (2016). Epithelial tricellular junctions act as interphase cell shape sensors to orient mitosis. Nature *530*, 495–498. https://doi.org/10.1038/nature16970.

59. Grosshans, J., and Wieschaus, E. (2000). A genetic link between morphogenesis and cell division during formation of the ventral furrow in Drosophila. Cell *101*, 523–531.

60. Seher, T.C., and Leptin, M. (2000). Tribbles, a cell-cycle brake that coordinates proliferation and morphogenesis during Drosophila gastrulation. Curr. Biol. *10*, 623–629.

61. Mata, J., Curado, S., Ephrussi, A., and Rørth, P. (2000). Tribbles coordinates mitosis and morphogenesis in Drosophila by regulating string/CDC25 proteolysis. Cell *101*, 511–522.

62. Knoblich, J.A., Sauer, K., Jones, L., Richardson, H., Saint, R., and Lehner, C.F. (1994). Cyclin E controls S phase progression and its down-regulation during Drosophila embryogenesis is required for the arrest of cell proliferation. Cell *77*, 107–120. https://doi.org/10.1016/0092-8674(94)90239-9.

63. Bergmann, A., Agapite, J., McCall, K., and Steller, H. (1998). The Drosophila gene hid is a direct molecular target of ras-dependent survival signaling. Cell *95*, 331–341. https://doi.org/10.1016/S0092-8674(00)81765-1.

64. Kurada, P., and White, K. (1998). Ras promotes cell survival in Drosophila by downregulating hid expression. Cell *95*, 319–329. https://doi.org/10.1016/S0092-8674(00)81764-X.

65. Regot, S., Hughey, J.J., Bajar, B.T., Carrasco, S., and Covert, M.W. (2014). High-sensitivity measurements of multiple kinase activities in live single cells. Cell *157*, 1724–1734. https://doi.org/10.1016/j.cell.2014.04.039.

66. Yuen, A.C., Prasad, A.R., Fernandes, V.M., and Amoyel, M. (2022). A kinase translocation reporter reveals real-time dynamics of ERK activity in Drosophila. Biol. Open *11*, https://doi.org/10.1242/BIO.059364.

67. Panciera, T., Azzolin, L., Cordenonsi, M., and Piccolo, S. (2017). Mechanobiology of YAP and TAZ in physiology and disease. Nat. Rev. Mol. Cell Biol. *18*, 758–770. https://doi.org/10.1038/nrm.2017.87.

68. Tapon, N., Harvey, K.F., Bell, D.W., Wahrer, D.C.R., Schiripo, T.A., Haber, D.A., and Hariharan, I.K. (2002). salvador promotes both cell cycle exit and apoptosis in Drosophila and is mutated in human cancer cell lines. Cell *110*, 467–478.

69. Harvey, K.F., Pfleger, C.M., and Hariharan, I.K. (2003). The Drosophila Mst ortholog, hippo, restricts growth and cell proliferation and promotes apoptosis. Cell *114*, 457–467.

70. Udan, R.S., Kango-Singh, M., Nolo, R., Tao, C., and Halder, G. (2003). Hippo promotes proliferation arrest and apoptosis in the Salvador/Warts pathway. Nat. Cell Biol. *5*, 914–920. https://doi.org/10.1038/ncb1050.

71. Huang, J., Wu, S., Barrera, J., Matthews, K., and Pan, D. (2005). The Hippo signaling pathway coordinately regulates cell proliferation and apoptosis by inactivating Yorkie, the Drosophila homolog of YAP. Cell *122*, 421–434. https://doi.org/10.1016/j.cell.2005.06.007.

72. Brennecke, J., Hipfner, D.R., Stark, A., Russell, R.B., and Cohen, S.M. (2003). bantam encodes a developmentally regulated microRNA that controls cell proliferation and regulates the proapoptotic gene hid in Drosophila. Cell *113*, 25–36. https://doi.org/10.1016/S0092-8674(03)00231-9.

73. Zhang, L., Ren, F., Zhang, Q., Chen, Y., Wang, B., and Jiang, J. (2008). The TEAD/TEF family of transcription factor Scalloped mediates Hippo signaling in organ size control. Dev. Cell *14*, 377–387. https://doi.org/10.1016/j.devcel.2008.01.006.

74. Matakatsu, H., and Blair, S.S. (2012). Separating planar cell polarity and Hippo pathway activities of the protocadherins fat and Dachsous. Development *139*, 1498–1508. https://doi.org/10.1242/dev.070367.

75. Das Thakur, M., Feng, Y., Jagannathan, R., Seppa, M.J., Skeath, J.B., and Longmore, G.D. (2010). Ajuba LIM proteins are negative regulators of the hippo signaling pathway. Curr. Biol. *20*, 657–662. https://doi.org/10.1016/j.cub.2010.02.035.

76. Reddy, B.V.V.G., and Irvine, K.D. (2013). Regulation of hippo signaling by EGFR-MAPK signaling through Ajuba family proteins. Dev. Cell *24*, 459–471. https://doi.org/10.1016/j.devcel.2013.01.020.

77. Rauskolb, C., Sun, S., Sun, G., Pan, Y., and Irvine, K.D. (2014). Cytoskeletal tension inhibits Hippo signaling through an Ajuba-Warts complex. Cell *158*, 143–156. https://doi.org/10.1016/j.cell.2014.05.035.

78. Battaglioni, S., Benjamin, D., Wälchli, M., Maier, T., and Hall, M.N. (2022). mTOR substrate phosphorylation in growth control. Cell *185*, 1814–1836. https://doi.org/10.1016/J.CELL.2022.04.013.

79. Baker, N.E. (2020). Emerging mechanisms of cell competition. Nat. Rev. Genet. *21*, 683–697. https://doi.org/10.1038/s41576-020-0262-8.

80. Vishwakarma, M., and Piddini, E. (2020). Outcompeting cancer. Nat. Rev. Cancer *20*, 187–198. https://doi.org/10.1038/s41568-019-0231-8.

81. Matamoro-Vidal, A., and Levayer, R. (2019). Multiple influences of mechanical forces on cell competition. Curr. Biol. *29*, R762–R774. https://doi.org/10.1016/j.cub.2019.06.030.

82. Johnston, L.A. (2009). Competitive interactions between cells: death, growth, and geography. Science *324*, 1679–1682. https://doi.org/10.1126/science.1163862.

83. Clavería, C., and Torres, M. (2016). Cell competition: mechanisms and physiological roles. Annu. Rev. Cell Dev. Biol. *32*, 411–439. https://doi.org/10.1146/ANNUREV-CELLBIO-111315-125142.

84. Nagata, R., and Igaki, T. (2018). Cell competition: emerging mechanisms to eliminate neighbors. Dev. Growth Differ. *60*, 522–530. https://doi.org/10.1111/DGD.12575.

85. Merino, M.M., Rhiner, C., Lopez-Gay, J.M., Buechel, D., Hauert, B., and Moreno, E. (2015). Elimination of unfit cells maintains tissue health and prolongs lifespan. Cell *160*, 461–476. https://doi.org/10.1016/j.cell.2014.12.017.

86. Lai, E.C. (2004). Notch signaling: control of cell communication and cell fate. Development *131*, 965–973. https://doi.org/10.1242/dev.01074.

87. Artavanis-Tsakonas, S., and Muskavitch, M.A.T. (2010). Notch: the past, the present, and the future. In Current Topics in Developmental Biology, (Elsevier). https://doi.org/10.1016/S0070-2153(10)92001-2.

88. Sjöqvist, M., and Andersson, E.R. (2019). Do as I say, Not(ch) as I do: lateral control of cell fate. Dev. Biol. *447*, 58–70. https://doi.org/10.1016/j.ydbio.2017.09.032.

89. Truman, J.W., Moats, W., Altman, J., Marin, E.C., and Williams, D.W. (2010). Role of Notch signaling in establishing the hemilineages of secondary neurons in Drosophila melanogaster. Development *137*, 53–61. https://doi.org/10.1242/dev.041749.

90. Bertet, C., Li, X., Erclik, T., Cavey, M., Wells, B., and Desplan, C. (2014). Temporal patterning of neuroblasts controls notch-mediated cell survival through regulation of hid or reaper. Cell *158*, 1173–1186. https://doi.org/10.1016/j.cell.2014.07.045.

91. Shaya, O., Binshtok, U., Hersch, M., Richardson, G.P., Chen, C.S., and Sprinzak, D. (2017). Cell-cell contact area affects Notch signaling and Notch-dependent patterning. Dev. Cell *40*, 505–511.e6. https://doi.org/10.1016/j.devcel.2017.02.009.

92. Djiane, A., Krejci, A., Bernard, F., Fexova, S., Millen, K., and Bray, S.J. (2013). Dissecting the mechanisms of Notch induced hyperplasia. EMBO J. *32*, 60–71. https://doi.org/10.1038/EMBOJ.2012.326.

93. Housden, B.E., Millen, K., and Bray, S.J. (2012). Drosophila reporter vectors compatible with ΦC31 integrase transgenesis techniques and their use to generate new notch reporter fly lines. G3 (Bethesda) *2*, 79–82. https://doi.org/10.1534/G3.111.001321.

94. Crawford, E.D., and Wells, J.A. (2011). Caspase substrates and cellular remodeling. Annu. Rev. Biochem. *80*, 1055–1087. https://doi.org/10.1146/ANNUREV-BIOCHEM-061809-121639.

95. Heisenberg, C.P., and Bellaïche, Y. (2013). Forces in tissue morphogenesis and patterning. Cell *153*, 948–962. https://doi.org/10.1016/j.cell.2013.05.008.

96. Hannezo, E., and Heisenberg, C.P. (2019). Mechanochemical feedback loops in development and disease. Cell *178*, 12–25. https://doi.org/10.1016/j.cell.2019.05.052.

97. McBeath, R., Pirone, D.M., Nelson, C.M., Bhadriraju, K., and Chen, C.S. (2004). Cell shape, cytoskeletal tension, and RhoA regulate stem cell lineage commitment. Dev. Cell *6*, 483–495. https://doi.org/10.1016/S1534-5807(04)00075-9.

98. Kilian, K.A., Bugarija, B., Lahn, B.T., and Mrksich, M. (2010). Geometric cues for directing the differentiation of mesenchymal stem cells. Proc. Natl. Acad. Sci. USA *107*, 4872–4877. https://doi.org/10.1073/PNAS.0903269107.

99. Mancini, L., Guirao, B., Ortica, S., Labusch, M., Cheysson, F., Bonnet, V., Phan, M.S., Herbert, S., Mahou, P., Menant, E., et al. (2023). Apical size and deltaA expression predict adult neural stem cell decisions along lineage progression. Sci. Adv. *9*, eadg7519. https://doi.org/10.1126/SCIADV.ADG7519.

100. Totaro, A., Panciera, T., and Piccolo, S. (2018). YAP/TAZ upstream signals and downstream responses. Nat. Cell Biol. *20*, 888–899. https://doi.org/10.1038/s41556-018-0142-z.

101. Davis, J.R., and Tapon, N. (2019). Hippo signalling during development. Development *146*, https://doi.org/10.1242/dev.167106.

102. Totaro, A., Castellan, M., Di Biagio, D., and Piccolo, S. (2018). Crosstalk between YAP/TAZ and notch signaling. Trends Cell Biol. *28*, 560–573. https://doi.org/10.1016/j.tcb.2018.03.001.

103. Engel-Pizcueta, C., and Pujades, C. (2021). Interplay between Notch and YAP/TAZ pathways in the regulation of cell fate during embryo development. Front. Cell Dev. Biol. *9*, 711531. https://doi.org/10.3389/fcell.2021.711531.

104. Valon, L., Davidović, A., Levillayer, F., Villars, A., Chouly, M., Cerqueira-Campos, F., and Levayer, R. (2021). Robustness of epithelial sealing is an emerging property of local ERK feedback driven by cell elimination. Dev. Cell *56*, 1700–1711.e8. https://doi.org/10.1016/j.devcel.2021.05.006.

105. Gagliardi, P.A., Dobrzyński, M., Jacques, M.A., Dessauges, C., Ender, P., Blum, Y., Hughes, R.M., Cohen, A.R., and Pertz, O. (2021). Collective ERK/Akt activity waves orchestrate epithelial homeostasis by driving apoptosis-induced survival. Dev. Cell *56*, 1712–1726.e6. https://doi.org/10.1016/J.DEVCEL.2021.05.007.

106. Wagstaff, L., Kolahgar, G., and Piddini, E. (2013). Competitive cell interactions in cancer: a cellular tug of war. Trends Cell Biol. *23*, 160–167. https://doi.org/10.1016/j.tcb.2012.11.002.

107. Nagata, R., Akai, N., Kondo, S., Saito, K., Ohsawa, S., and Igaki, T. (2022). Yorkie drives supercompetition by non-autonomous induction of autophagy via bantam microRNA in Drosophila. Curr. Biol. *32*, 1064–1076.e4. https://doi.org/10.1016/J.CUB.2022.01.016.

108. Alcolea, M.P., and Jones, P.H. (2015). Cell competition: winning out by losing notch. Cell Cycle *14*, 9–17. https://doi.org/10.4161/15384101.2014.988027.

109. Neto-Silva, R.M., de Beco, S., and Johnston, L.A. (2010). Evidence for a growth-stabilizing regulatory feedback mechanism between Myc and Yorkie, the drosophila homolog of Yap. Dev. Cell *19*, 507–520. https://doi.org/10.1016/j.devcel.2010.09.009.

110. Ziosi, M., Baena-López, L.A., Grifoni, D., Froldi, F., Pession, A., Garoia, F., Trotta, V., Bellosta, P., Cavicchi, S., and Pession, A. (2010). dMyc functions downstream of Yorkie to promote the supercompetitive behavior of Hippo pathway mutant cells. PLoS Genet. *6*, e1001140. https://doi.org/10.1371/JOURNAL.PGEN.1001140.

111. Oda, H., Tsukita, S., and Takeichi, M. (1998). Dynamic behavior of the cadherin-based cell–cell adhesion system during Drosophila gastrulation. Dev. Biol. *203*, 435–450.

112. Huang, J., Zhou, W., Dong, W., Watson, A.M., and Hong, Y. (2009). From the cover: directed, efficient, and versatile modifications of the Drosophila genome by genomic engineering. Proc. Natl. Acad. Sci. USA *106*, 8284–8289. https://doi.org/10.1073/pnas.0900641106.

113. Pinheiro, D., Hannezo, E., Herszterg, S., Bosveld, F., Gaugue, I., Balakireva, M., Wang, Z., Cristo, I., Rigaud, S.U., Markova, O., et al. (2017). Transmission of cytokinesis forces via E-cadherin dilution and actomyosin flows. Nature *545*, 103–107. https://doi.org/10.1038/nature22041.

114. Gracia, M., Theis, S., Proag, A., Gay, G., Benassayag, C., and Suzanne, M. (2019). Mechanical impact of epithelial−mesenchymal transition on epithelial morphogenesis in Drosophila. Nat. Commun. *10*, 2951. https://doi.org/10.1038/s41467-019-10720-0.

115. Sabino, D., Brown, N.H., and Basto, R. (2011). Drosophila Ajuba is not an Aurora-A activator but is required to maintain Aurora-A at the centrosome. J. Cell Sci. *124*, 1156–1166. https://doi.org/10.1242/jcs.076711.

116. Neufeld, T.P., de la Cruz, A.F., Johnston, L.A., and Edgar, B.A. (1998). Coordination of growth and cell division in the Drosophila wing. Cell *93*, 1183–1193. https://doi.org/10.1016/S0092-8674(00)81462-2.

117. di Pietro, F., Herszterg, S., Huang, A., Bosveld, F., Alexandre, C., Sancéré, L., Pelletier, S., Joudat, A., Kapoor, V., Vincent, J.P., et al.

(2021). Rapid and robust optogenetic control of gene expression in Drosophila. Dev. Cell *56*, 3393–3404.e7. https://doi.org/10.1016/j.devcel.2021.11.016.

118. Brand, A.H., and Perrimon, N. (1993). Targeted gene expression as a means of altering cell fates and generating dominant phenotypes. Development *118*, 401–415.

119. McGuire, S.E., Le, P.T., Osborn, A.J., Matsumoto, K., and Davis, R.L. (2003). Spatiotemporal rescue of memory dysfunction in Drosophila. Science *302*, 1765–1768. https://doi.org/10.1126/science.1089035.

120. Golic, K.G., and Lindquist, S. (1989). The FLP recombinase of yeast catalyzes site-specific recombination in the drosophila genome. Cell *59*, 499–509. https://doi.org/10.1016/0092-8674(89)90033-0.

121. Xu, T., and Rubin, G.M. (1993). Analysis of genetic mosaics in developing and adult Drosophila tissues. Development *117*, 1223–1237. https://doi.org/10.1242/dev.117.4.1223.

122. Fichelson, P., and Gho, M. (2004). Mother-daughter precursor cell fate transformation after Cdc2 down-regulation in the Drosophila bristle lineage. Dev. Biol. *276*, 367–377. https://doi.org/10.1016/J.YDBIO.2004.08.043.

123. Ségalen, M., Johnston, C.A.C.A., Martin, C.A., Dumortier, J.G.J.G., Prehoda, K.E.K.E., David, N.B.N.B., Doe, C.Q.C.Q., and Bellaïche, Y. (2010). The Fz-Dsh planar cell polarity pathway induces oriented cell division via Mud/NuMA in drosophila and zebrafish. Dev. Cell *19*, 740–752. https://doi.org/10.1016/j.devcel.2010.10.004.

124. Li, M.Z., and Elledge, S.J. (2012). SLIC: a method for sequence- and ligation-independent cloning. Methods Mol. Biol. *852*, 51–59. https://doi.org/10.1007/978-1-61779-564-0_5.

125. Figard, L., and Sokac, A.M. (2011). Imaging cell shape change in living Drosophila embryos. J. Vis. Exp. 2503.

126. Fink, J., Carpi, N., Betz, T., Bétard, A., Chebah, M., Azioune, A., Bornens, M., Sykes, C., Fetler, L., Cuvelier, D., et al. (2011). External forces control mitotic spindle positioning. Nat. Cell Biol. *13*, 771–778. https://doi.org/10.1038/ncb2269.

127. Arthur, D., and Vassilvitskii, S. (2006). k-means++: the advantages of careful seeding. In Proceedings of the Eighteenth Annual ACM-Siam Symposium on Discrete Algorithms, pp. 1027–1035.

128. Weigert, M., Schmidt, U., Boothe, T., Müller, A., Dibrov, A., Jain, A., Wilhelm, B., Schmidt, D., Broaddus, C., Culley, S., et al. (2018). Content-aware image restoration: pushing the limits of fluorescence microscopy. Nat. Methods *15*, 1090–1097. https://doi.org/10.1038/s41592-018-0216-7.

129. Schmidt, U., Weigert, M., Broaddus, C., and Myers, G. (2018). Cell detection with star-convex polygons. International Conference on Medical Image Computing and Computer-Assisted Intervention. Medical Image Computing and Computer Assisted Intervention – MICCAI 2018. Lecture Notes in Computer Science (including subseries Lecture Notes in Artificial Intelligence and Lecture Notes in Bioinformatics) *11071*, 265–273. https://doi.org/10.1007/978-3-030-00934-2_30.

130. Arganda-Carreras, I., Kaynig, V., Rueden, C., Eliceiri, K.W., Schindelin, J., Cardona, A., and Sebastian Seung, H.S. (2017). Trainable Weka Segmentation: a machine learning tool for microscopy pixel classification. Bioinformatics *33*, 2424–2426. https://doi.org/10.1093/BIOINFORMATICS/BTX180.

131. Herbert, A.D., Carr, A.M., and Hoffmann, E. (2014). FindFoci: a focus detection algorithm with automated parameter training that closely matches human assignments, reduces human inconsistencies and increases speed of analysis. PLOS One *9*, e114749. https://doi.org/10.1371/journal.pone.0114749.

132. Ghasemi, A., and Zahediasl, S. (2012). Normality tests for statistical analysis: a guide for non-statisticians. Int. J. Endocrinol. Metab. *10*, 486–489. https://doi.org/10.5812/IJEM.3505.

133. Lumley, T., Diehr, P., Emerson, S., and Chen, L. (2002). The importance of the normality assumption in large public health data sets. Annu. Rev. Public Health *23*, 151–169. https://doi.org/10.1146/ANNUREV.PUBLHEALTH.23.100901.140546.

134. Kwak, S.G., and Kim, J.H. (2017). Central limit theorem: the cornerstone of modern statistics. Korean J. Anesthesiol. *70*, 144–156. https://doi.org/10.4097/KJAE.2017.70.2.144.

Please cite this article in press as: Cachoux et al., Epithelial apoptotic pattern emerges from global and local regulation by cell apical area, Current Biology (2023), https://doi.org/10.1016/j.cub.2023.09.049

STAR★METHODS

KEY RESOURCES TABLE

REAGENT or RESOURCE	SOURCE	IDENTIFIER
Experimental models: Organisms/strains		
Drosophila: Ubi-Ecad:GFP	Oda et al.[111]	NA
Drosophila: Ecad:GFP	Huang et al.[112]	NA
Drosophila: Ecad:3xGFP	Pinheiro et al.[113]	NA
Drosophila: Ecad:3xmKate2	Pinheiro et al.[113]	NA
Drosophila: Ecad:3xTagRFP	Pinheiro et al.[113]	NA
Drosophila: sqh:3xGFP	Pinheiro et al.[113]	NA
Drosophila: sqh:mTagRFP	Garcia et al.[114]	NA
Drosophila: jub:GFP	Sabino et al.[115]	BDSC #56806
Drosophila: Ubi-nls:RFP FRT19A	Bloomington Drosophila Stock Center	BDSC #31416
Drosophila: FRT40A Ubi-nls:GFP	Bloomington Drosophila Stock Center	BDSC #5189
Drosophila: UAS-CycE^{18}; UAS-CycE	Neufeld et al.[116]; gift from Michel Gho	NA
Drosophila: UAS-trbl	Grosshans and Wieschaus[59]	NA
Drosophila: UAS-Diap1	Bloomington Drosophila Stock Center	BDSC #6657
Drosophila: UAS-w^{dsRNA}	VDRC Stock Center	VDRC#33034
Drosophila: UAS-Tor^{dsRNA}	Bloomington Drosophila Stock Center	BDSC#34639
Drosophila: UAS-RHG^{dsRNA}	Pinheiro et al.[113]; gift from Marco Milan	NA
Drosophila: UAS-Actn^{dsRNA}	Bloomington Drosophila Stock Center	BDSC#34874
Drosophila: UAS-jub^{dsRNA}	Bloomington Drosophila Stock Center	BDSC#41938
Drosophila: UAS-Ras^{V12}	Bloomington Drosophila Stock Center	BDSC#64196
Drosophila: UAS-Notch^{dsRNA}	Bloomington Drosophila Stock Center	BDSC#7078
Drosophila: w^{117}		NA
Drosophila: azot^{KO}	Merino et al.[85];gift from Eduardo Moreno	NA
Drosophila: N$^{l1N\text{-}ts1}$	Bloomington Drosophila Stock Center	BDSC#2533
Drosophila: Ubi-KTR:GFP	This study.	NA
Drosophila: NRE-nls:mChFP	Housden et al.[93]	NA
Drosophila: ban-nls:GFP	Matakastu and Blair[74]	NA
Drosophila: UAS-GC3Ai	Schott et al.[50]	NA
Drosophila: Diap1$^{3.5}$-GFP	Zhang et al.[73]	NA
Drosophila: Diap1$^{4.3}$-GFP	Zhang et al.[73]	NA
Drosophila: Ubi-His2B:RFP	Bosveld et al.[42]	NA
Drosophila: Ubi-PH:GFP	Gift from F. Pichaud	NA
Drosophila: hs-flp	Bloomington Drosophila Stock Center	BDSC#8862
Drosophila: Act>CD2>Gal4, UAS-Caax:tBFP	Lopez et al.[43]	NA
Drosophila: Act-Gal4	Bloomington Drosophila Stock Center	BDSC#3954
Drosophila: Pnr-Gal4	Bloomington Drosophila Stock Center	BDSC#29650
Drosophila: tub-GAL80^{ts}	Bloomington Drosophila Stock Center	BDSC#7017
Drosophila: Ubi-2xpMagHigh1:AD	di Pietro et al.[117]	BDSC#94197
Drosophila: Ubi-Gal4DBD:2xnMagHigh1	di Pietro et al.[117]	BDSC#94198
Chemicals		
DPBS	PAN Biotech	Cat#P04-36010P
Triton	Sigma-Aldrich	Cat#9002-93-1
PFA 16% Aqueouse SOL	Electron Microscopy Science	Cat#15710
DAPI	Sigma-Aldrich	Cat#D9542

(*Continued on next page*)

Please cite this article in press as: Cachoux et al., Epithelial apoptotic pattern emerges from global and local regulation by cell apical area, Current Biology (2023), https://doi.org/10.1016/j.cub.2023.09.049

Continued

REAGENT or RESOURCE	SOURCE	IDENTIFIER
Antibodies		
Rabbit anti-dpERK	Cell Signaling	Cat#4370
Chicken anti-GFP	Abcam	Cat#13970
Donkey anti-rabbit Cy3	Jackson Immunoresearch	Cat#711-165-152
Donkey anti-chicken Alexa488	Jackson Immunoresearch	Cat#703-545-155
Software and algorithms		
Fiji	http://fiji.sc	SCR_002285
MetaMorph Microscopy Automation and Image Analysis Software	Molecular devices http://www.moleculardevices.com/Products/Software/Meta-Imaging-Series/MetaMorph.html	SCR_002368
ZEN Digital Imaging for Light Microscopy	Zeiss http://www.zeiss.com/microscopy/en_us/products/microscope-software/zen.html#introduction	SCR_013672
Matlab	Mathworks http://www.mathworks.com/products/matlab/	SCR_001622

RESOURCE AVAILABILITY

Lead contact

Further information and requests for resources and reagents should be directed to, and will be fulfilled by the lead contact, Yohanns Bellaïche (yohanns.bellaiche@curie.fr).

Materials availability

All unique/stable reagents generated in this study are available from the lead contact without restriction.

Data and code availability

- All original microscopy data reported in this paper will be shared by the lead contact upon request.
- This paper report original codes available from the lead contact upon request.
- Any additional information required to reanalyse the data reported in this paper is available from the lead contact upon request.

EXPERIMENTAL MODEL AND SUBJECT DETAILS

Fly husbandry and stocks

Flies were grown on standard cornmeal/yeast food at 18°C or 25°C, and experiments were performed at 25° unless otherwise specified. *Drosophila melanogaster* stocks used in this study and associated references are listed in the key resources table.

METHOD DETAILS

Genetics

Genotypes used in each figure panel are listed in Table S2. Loss-of-function and gain-of-function experiments were carried out using the Gal4/UAS system utilizing the temperature sensitive Gal80^{ts}.[118,119] To tune the transcriptional activity of the *Act-GAL4* drivers, animals were raised at 18°C and incubated at 29°C before mounting at head eversion (12 hAPF) for 4 h (UAS-*CycE*) or 24 h (UAS-*trbl*). For clonal loss-of-function analyses the FLP/FRT flip-out system was employed using the Act>CD2>Gal4, UAS-Caax:tBFP line to express Gal4 and labelled the clones by membrane localized BFP.[120,121] Larvae were raised at 25°C, somatic clones were induced in the third instar larval stage by heat shock at 37°C for 10 min (UAS-*Ras*^{V12}, UAS-*Notch*^{dsRNA}, UAS-*Tor*^{dsRNA}, UAS-*diap1*, UAS-*RHG*^{dsRNA}) or 20 min (UAS-*jub*^{dsRNA},UAS-*Actn*^{dsRNA}) and then incubated at 29°C for 24 h (UAS-*Ras*^{V12}, UAS-*Notch*^{dsRNA}, UAS-*Tor*^{dsRNA}) or 48 h (UAS-*trbl*, UAS-*RHG*^{dsRNA},UAS-*jub*^{dsRNA},UAS-*Actn*^{dsRNA}) before mounting. To tune Notch activity, *Notch*^{ts} animal were raised at 18°C, and *Notch*^{ts}/Y male pupae were selected and then shifted to 29°C 3 hours prior to imaging. Upon imaging, quantitative analyses were performed in pupa that exhibited an absence of external sensory organs confirming the loss of Notch activity.[122] Analysis of Caspase activation in *Notch*^{ts} context was done using the ShineGal4 (ubi-Gal4^{MagHigh}) system[117] to drive the GC3Ai Caspase activity reporter: animals were raised in the dark and exposed to daylight 1 day before mounting.

Please cite this article in press as: Cachoux et al., Epithelial apoptotic pattern emerges from global and local regulation by cell apical area, Current Biology (2023), https://doi.org/10.1016/j.cub.2023.09.049

Generation of ERK KTR:GFP transgenic reporter

The Ubi-*KTR:GFP* reporter was generated by cloning the KTR:GFP sequence[65] in a modified pUbi vector[123] using SLIC.[124] All embryo transgenesis injections were performed by Bestgene and transgenes were confirmed by PCR and sequencing. Detailed plasmid maps and their DNA sequences are available upon request.

Pupa and adult mounting and imaging

Pupal notum dissection, fixation, staining, and imaging

Upon removal of the pupal case, pupae were glued on their dorsal side to a 20 mm glass bottom microwell dish (MatTek Life Sciences) using heptane glue.[125] Pupal nota were then dissected, fixed and stained into MatTek glass bottom dish. Briefly, the nota were dissected in PBS, fixed in 4% formaldehyde solution, permeabilised/washed in PBT 0.4% triton, stained with primary antibody solution washed and then stained with secondary antibody solution. Primary antibodies used: rabbit anti-dpERK (Cell signalling, #4370, 1/100), chicken anti-GFP (Abcam, #13970, 1/500). Secondary antibodies used: donkey anti-rabbit Cy3 and donkey anti-chicken Alexa488 (Jackson Immunoresearch). Dissected nota were mounted in 80% glycerol with n-propyl galate with DAPI (Sigma-Aldrich). They were imaged using an inverted confocal spinning disk Carl Zeiss microscope using 40x/1.4 OIL DIC H/N2 PL FLUOR and sCMOS camera (Orca Flash4, Hamamatsu). Images shown are maximal (dpERK and DAPI) or average (KTR:GFP) z-projections.

Time-lapse live imaging

Notum live imaging was performed as described previously.[40,113] Pupae were collected at the white pupae stage (0 hAPF) and mounted after head eversion (12 hAPF). Samples were imaged with an inverted confocal spinning disk Carl Zeiss or Nikon microscopes using 40x/1.4 OIL DIC H/N2 PL FLUOR, 60x/1.4 OIL PL APO, 63x/1.4 OIL DICII PL APO VC objectives and a sCMOS camera (Orca Flash4, Hamamatsu). Unless otherwise stated, all movies were acquired at 29°C using tile imaging (6 to 10 tiled positions), z stacks (0.5 μm/slice over 12.5 or 13.5 μm), every 5 min using autofocus. The autofocus was performed using the Ecad fluorescent signal.

Compaction of Drosophila notum and imaging

White pupae (0 hAPF) were collected with a wet paintbrush and placed on double-side tape with a coverslip on top of the pupae to flatten the notum and ease the later compaction. In parallel, a 3.5 by 1 cm polydimethylsiloxane (PDMS – from Gel Pack: Gel Film PF_60_x4) stripe was attached to a custom-made compaction device and pre-stretched to 150%.[43,126] After 15h30 to 16h30 of development at 25°C, the pupal cases were fully removed and the flattened pupae were carefully grabbed by the head with a plastic tip to be glued, with heptane glue, on the pre-stretched PDMS. For live-imaging, the compaction device was fixed to the stage of an inverted confocal spinning disk Nikon microscope and pupae were imaged at 25°C with an 40x NA 0.95 Air dry PL APO objective. In the case of compacted pupae, using the micrometric screw of the compaction device, the pre-stretched PDMS was progressively released over 30 minutes to carry out a ~15% uniaxial compaction. At each step, a confocal z stack (15 slices, 0.5μm/slice) was taken to follow the tissue dynamics during compaction. Then, image acquisition was performed until 30 hAPF by acquiring z stacks (15 slices, 0.5μm/slice) every 5 min with autofocus performed using the Ecad fluorescent signal.

Prediction model

Design and training of a prediction model

To build a prediction model, segmented data from 6 developing heminota were used as a training and validation dataset. The prediction dataset consisted in the data from 3 heminota. Cells whose future fate was known were selected, and their area and relative area were averaged over their pre-extrusion phases, to avoid the bias induced by the drastic cell shape changes happening at the end of a cell life. For each cell, these average geometrical features were normalized and the Euclidian distance to mean values was computed to detect and remove the 0.5% outliers. Using this data, we constructed a k-means clustering-inspired prediction model. To create clusters, initial values were chosen using the k-means++ algorithm.[127] The clusters were then optimized through an iterative process so as to get clusters with a constant number of cells $n_{cluster}$. For each cluster, the rate of apoptotic cells was calculated. The optimal size of clusters $n_{cluster}$ and prediction threshold p_{thresh} were estimated using a grid search and k-fold cross-validation with 5 subsets. The F1-score was used as a scoring metrics as it is more appropriate when working with imbalanced datasets. Additional model types were tested: the random forest and logistic regression from the scikit-learn machine learning library in Python. Both were less successful than the clustering model (F1-scores: clustering model, 0.55; random forest, 0.50; logistic regression, 0.39; random model, 0.14).

Prediction steps using the clustering prediction model

In the prediction phase, the data from segmented nota is pre-processed similarly to that of the training dataset (the area and relative area are averaged over the cell pre-extrusion phase and normalized with the same normalization parameters as the training data). Each cell is then assigned to its closest cluster depending on its geometrical features and is attributed the corresponding apoptosis rate. Cells whose apoptosis rate is higher than the threshold p_{thresh} are predicted to die.

Prediction of the impact of tissue compaction on cell apoptosis

To test how experimental tissue compaction would impact the apoptosis rate, we extracted the segmented data from 3 non-compacted nota. This data was pre-processed as in the standard prediction phase (averaged and normalized), except that the average apical area of each cell was decreased by 19% before normalization. The average relative apical areas were kept unchanged. We then ran the clustering prediction model on this compacted cell data to obtain predicted apoptosis over the scutellum.

Please cite this article in press as: Cachoux et al., Epithelial apoptotic pattern emerges from global and local regulation by cell apical area, Current Biology (2023), https://doi.org/10.1016/j.cub.2023.09.049

QUANTIFICATION AND STATISTICAL ANALYSIS

Quantifications of tissue dynamics

Unless otherwise stated, all images and movies are maximal *z*-projections. Movies were restored and projected using the CARE deep neural network.[128]

Spatial and temporal registration of time-lapse movies

Between 14-17 hAPF the presumptive neck-thorax boundary, the macrochaetae of the notum and the a-p axis provide reproducible spatial landmarks easily identifiable using apical junction markers such as Ecad:3xGFP. We used their positions before 18 hAPF to register all time-lapse movies in space. To register time-lapse movies in time, the maximum of the tissue rotation rate in a reference window was used as described in [39,40]. To correct for the difference in developmental time between 25°C and 29°C, a correction factor of 1.11 was applied to data acquired at 29°C to match the 25°C timing. Note that each experimental condition was compared to a control condition acquired at the same temperature, so this correction factor does not impact any of our conclusions. Experimental conditions and their associated controls were analysed over the largest developmental time window that was common to all the corresponding animals.

Segmentation and tracking

Cell apical junction labelled by Ecad fluorescent signal were segmented using our own segmentation software based on watershed and on the StarDist deep neural network[129] as described in [117]. Cell tracking was performed using MATLAB and C++ codes as previously described[39,40] to identify cell divisions and extrusions. We thereby obtained cell apical area at a given timepoint in a given image using MATLAB function “regionprops” (image processing toolbox) that extracts the number of pixels within each segmented cell (as well as many other geometric features). Our cell tracking software then enabled to follow individual cells and their geometric features, extracted as described above, over time. For clonal analysis the tissue contralateral regions which are symmetric with respect to the midline to clones of interest were used as control. These contralateral regions were rigorously defined based on the positions of the macrochaetae and midline. The contralateral symmetric regions were defined at the first frame of the movies, then the corresponding cells were tracked over time.

Apoptosis mask

To create a mask of apoptosis at the notum scale, we used the grey level maps of the offspring apoptotic rates (as shown in Figure 1C) for 5 heminota, taken at the same time points. Three masks were created, at 15 hAPF, 17h30 APF and 20 hAPF, to adapt for movies with different starting times. The grey level maps were binarized and a Gaussian blur was applied using Fiji with a sigma (radius) of 5 pixels. The maps were then rescaled so that the origin and spatial landmarks of all maps would match.[39] The 5 rescaled maps were superimposed on one another, and the resulting map was blurred (Gaussian blur with a sigma of 20 pixels) to visualize the coarse-grained regions of apoptosis. The boundaries between regions were then drawn manually.

Fold-change in apoptosis rate

The fold-change in apoptosis rate between two conditions (compacted versus non-compacted tissues, or mutant versus control) was calculated as the ratio of the apoptosis rates of these two conditions: (apoptosis rate in compacted)/(apoptosis rate in non-compacted) or (apoptosis rate in mutant)/(apoptosis rate in control), respectively.

Apoptosis clusters

To quantify the occurrence of apoptosis clusters, movies were segmented and tracked as described above. For every apoptosis, we then registered all the subsequent apoptosis occurring in a 5 μm-radius circular region around the apoptotic cell. We listed the elapsed times between the initial apoptosis and the subsequent neighboring ones. These elapsed times were concatenated for all the animals. Finally, the probability density estimate of elapsed times between neighboring apoptosis was calculated using the kernel smoothing *ksdensity()* MATLAB function with a restriction to positive values.

Measurements of tissue physiological contraction

To measure tissue contraction, tissue regions were segmented and the groups of cells making up each of these regions were then tracked over time as described above. A region area was measured as the sum of the areas of the segmented cells making up this region at each time step and then smoothed using a moving average. The moving average was performed over 2h-wide sliding time windows, with a 96%-overlap between successive time windows so that the time step between two windows is the same as the movie time frame. Finally, the smoothed region area was then normalized so that its maximum value over time equals one.

Measurement of area variation

The area variation is measured as the ratio between the initial area and the final one. To assess the variations of area during the 30 min where a compaction is artificially applied, in compacted, or not, in non-compacted, we are calculating as following: (final area – initial area)/initial area.

Quantification of fluorescent reporter

KTR:GFP fluorescent reporter and GC3Ai fluorescent sensor

All images and movies of the KTR:GFP reporter and GC3Ai sensor average z-projections of 20x0.5μm slices containing (centred on) nucleus plane are shown. To quantify Caspase activity in cells, we first average the GC3Ai sensor intensity in the cell region defined by cell segmentation at each time point. The GC3Ai intensity over time was smoothed using a moving median over 2 successive time frames; the differential of this GC3Ai signal was then used as a proxy for Caspase activity,[104] and calculated as the signal difference between successive frames. To quantify the apical area and relative apical area of cells expressing the KTR:GFP reporter, manual

Please cite this article in press as: Cachoux et al., Epithelial apoptotic pattern emerges from global and local regulation by cell apical area, Current Biology (2023), https://doi.org/10.1016/j.cub.2023.09.049

segmentation was performed using Fiji. Cells were segmented in their apical plane over several time points corresponding to half an hour, then these values were averaged. To quantify ERK activity in cells, at each time, we located the centre of the cell nuclei. At each z stack, a nucleus mask was defined, consisting in a 7 pixel-diameter circle centred on the nucleus centre. ERK activity was calculated as the ratio between cytoplasmic and nuclear ERK signals.[65] Nuclear ERK was calculated as the average ERK signal of all the pixels in the nucleus mask in the first 4 z-stacks on which the nucleus is clearly visible. Cytoplasmic ERK was calculated in the same manner in the 4 z stacks directly above the nucleus, just before the nucleus is visible.

ban-nls:GFP and Diap1-nls:GFP reporter

To quantify ban-nls:GFP in compacted and non-compacted tissue, ban-nls:GFP fluorescence quantifications were performed at 20h30 APF on maximum z-projections (15x0.5μm slices) located around the nucleus position. Then, the posterior medial notum region of each pupa was divided in 9 boxes to allow the comparison of similar region between compacted and non-compacted pupae. Upon segmentation of the nucleus using Fiji Trainable Weka segmentation,[130] the fluorescence intensity of the nucleus of each cell was measured in each box and compared between the two conditions.

To quantify ban-nls:GFP and Diap1-nls:GFP signal intensities in w^{RNAi} and $Notch^{RNAi}$ clones marked by the accumulation of Caax:BFP, clone outlines and the midline position were manually drawn in Fiji on each nota at 24–26 hAPF. Symmetric contralateral regions were then automatically determined using a custom-made Fiji plugin that exclude overlapping control and clonal regions. Average intensities were then determined in each clone and contralateral regions using Fiji Measure function. Average intensity within w^{RNAi} and $Notch^{RNAi}$ clones were normalized by the average intensity in the corresponding symmetric contralateral region. Clones of less than 6 cells were excluded to ensure sufficient reduction of protein function upon RNAi induction.

NRE-nls:mCherryFP *and* **Ubi-nls:RFP** *reporters*

To quantify NRE-nls:mCherryFP and Ubi-nls:RFP fluorescence intensities in notum cells, quantifications were performed at 26 hAPF on maximum z-projections located around the nucleus position. We located the centre of the cell nuclei and averaged reporter intensity in a 8 pixel-diameter circle centred on the nucleus centre. Notch activity was then normalized using a min-max normalization on the 0.1 and 99.9 percentiles; i.e., the reporter signal intensity corresponding to these percentiles were set to 0 and 1 respectively. To quantify cell relative apical area, we used our automated segmentation pipeline (see *Segmentation and Tracking* above).

Jub clustering in non-apoptotic and future apoptotic cells

To determine the ratio of Jub integrated intensity in clusters relative to the one elsewhere along the junction (ratio$^{in/out}$ of cluster), z-stack of single cells expressing Jub:GFP were sum-projected using Ecad:3xmKate2 signal (5 z-slices centred around the AJs and corresponding to 2 μm). Three fluorescent intensity measurements were then performed: (i) The mean fluorescent intensity in cluster (*Ic*): Clusters were automatically identified using the Fiji FindFoci plugin[131] using the following parameters: background:3; search:0.2; search method: Fraction of peak – background; peak:0.2; maximum peaks:50; fraction:0.50; minimumsize:5. The resulting mask was used to measure the intensity in each cluster (*Ic*) and the area occupied by each cluster (*Ac*); (ii) The total integrated intensity along the AJ, (*Iaj*): the AJ cell contour was selected using Fiji segmented line tool and used to measure (*Iaj*) and the total area of the cell junction (*Aaj*) and; (iii) The fluorescent background intensity (*Ib*) was measured by selecting the apical medial region of the cells and measuring the average intensity level. The signal in cluster was defined as $in^{cluster} = \frac{\sum_{each\ cluster}((Ic - Ib)*Ac)}{(Iaj - Ib)*Aaj}$ and the signal on the junction as $out^{cluster} = 1 - in^{cluster}$.The ratio$^{in/out}$ of cluster as $\frac{in^{cluster}}{out^{cluster}}$. Measurements were performed in the posterior medial domain of the tissue where aSF form. Measurements were made in future apoptotic cells 3h prior to their extrusion and in surrounding non-apoptotic at the same time point.

Statistics

Sample sizes vary in each experiment and animal samples were randomly selected within a given genotype for subsequent analyses. Experiments were repeated at least twice. Only animals correctly mounted for microscopy and without developmental delay were included in the analyses. The numbers of analysed animals and cells are indicated in the figures or their legends. For all graphs, each error bar/error area represents the standard error to the mean (SEM), unless specified otherwise. The statistical tests used to assess significance are stated in the figure legends or in the main text. Statistical analyses were performed using MATLAB and p values are given with a 5%-level of significance. To compare the time-evolutions of relative apical areas of apoptotic cells between two conditions or with an average at 1, time-evolutions of cells were first synchronized to their time of death and averaged, then, a two-sample Student's t-test was performed every 15 minutes and the associated p value was plotted as a horizontal bar on top of each graph (white: $p \geq 0.05$, light color: $p<0.05$ and dark color: $p<0.01$; dark color: same as the corresponding plot average line, light color: color of the SEM range). Comparison of two distributions were performed using a two-sample Student's t-test, Mann-Whitney U-test or Kolmogorov-Smirnov test as indicated in the figure legends. The Student's t-test was used for samples larger than 100 data points[132,133]; for such large samples, the normality assumption becomes unnecessary thanks to the Central Limit Theorem.[134] In Figure 5D, SEM for the experimental ratio in apoptosis rates between compacted and non-compacted pupae was calculated by using statistics of Bernoulli distributions. The probability to undergo apoptosis for compacted and non-compacted pupae (p_c and p_{nc}, respectively) is first estimated using the ratios of cells that underwent apoptosis (n) over the total number of cells (N): p = n/N. Then, given the large size of our samples (N_c = 4055 and N_{nc} = 4617), the distribution of error around p can be approximated by a normal distribution (central limit theorem) and the SEM can be estimated by $s = (p(1-p)/N)^{1/2}$ for each group (compacted and non-compacted). Then, to estimate the SEM of the ratio p_c/p_{nc}, since we also have $s/p << 1$ in each group, one can make a Taylor

Please cite this article in press as: Cachoux et al., Epithelial apoptotic pattern emerges from global and local regulation by cell apical area, Current Biology (2023), https://doi.org/10.1016/j.cub.2023.09.049

expansion at first order, which leads the SEM estimate for the ratio $s_{n/nc} = p_c/p_{nc}\,[((1\text{-}p_c)/(N_c\,p_c))^{1/2} + ((1\text{-}p_{nc})/(N_{nc}\,p_{nc}))^{1/2}]$. In Figure 7C, to determine whether the difference in relative area between either (i) R1 and R2 (their "R1/R2" ratio of mean relative area being 1.09 ± 0.01) or (ii) *Tor*^{RNAi} bulk and border cells (their "bulk/border" ratio of mean relative area being 1.14 ± 0.03) had an impact on cell apoptosis regardless of any differences in areas between either (i) R1 and R2 (their "R1/R2" ratio of mean areas being 1.09 ± 0.03 or (ii) between *Tor*^{RNAi} bulk and border cells (their "bulk/border" ratio of mean areas being 1.01 ± 0.05), two statistical logistic models were performed for each dataset (i.e., comparison R1 vs R2, and *Tor*^{RNAi} bulk vs border), one with area only, and one with area and relative area. A likelihood ratio statistic was then used to compare the models and determine whether relative area had significant impact on apoptosis. In Figure 7H, probability density of subsequent apoptosis times in *Notch*^{ts} tissues were performed using a Fisher test.